LEVEL II

12

REPORT NO. FR-81-23-636

AD A103483

AIRCRAFT TARGET VIEW DETERMINATION FOR METHOD OF MOMENTS IDENTIFICATION

GEORGE A. IOANNIDIS
ARIE BERMAN
CHARLES P. DOLAN
ADVANCED PROGRAMS DIVISION
RADAR SYSTEMS GROUP
HUGHES AIRCRAFT COMPANY
EL SEGUNDO, CA 90245

JUNE 1981

FINAL REPORT FOR PERIOD OCTOBER 1980 - JUNE 1981

APPROVED FOR PUBLIC RELEASE;
DISTRIBUTION UNLIMITED

Submitted to:
OFFICE OF NAVAL RESEARCH
ARLINGTON, VA 22217

DTIC FILE COPY

RADAR SYSTEMS GROUP

HUGHES

DTIC
ELECTE
AUG 31 1981
S D
D

81 8 31 167

UNCLASSIFIED

SECURITY CLASSIFICATION OF THIS PAGE (When Data Entered)

REPORT DOCUMENTATION PAGE	READ INSTRUCTIONS BEFORE COMPLETING FORM
1. REPORT NUMBER	2. GOVT ACCESSION NO. AD-A103 483	3. RECIPIENT'S CATALOG NUMBER
4. TITLE (and Subtitle) AIRCRAFT TARGET VIEW DETERMINATION FOR METHOD OF MOMENTS IDENTIFICATION	5. TYPE OF REPORT & PERIOD COVERED Final Report Oct. 1980 – June 1981
	6. PERFORMING ORG. REPORT NUMBER FR-81-23-836
7. AUTHOR(s) George A. Ioannidis Arie Berman, Charles P. Dolan	8. CONTRACT OR GRANT NUMBER(s) N00014-80-C-0940
9. PERFORMING ORGANIZATION NAME AND ADDRESS Hughes Aircraft Co., Advanced Programs Division, Radar Systems Group 2000 East Imperial Hwy, El Segundo, CA 90245	10. PROGRAM ELEMENT, PROJECT, TASK AREA & WORK UNIT NUMBERS
11. CONTROLLING OFFICE NAME AND ADDRESS Office of Naval Research Department of the Navy 800 N. Quincy Street, Arlington, VA 22217	12. REPORT DATE June 1981
	13. NUMBER OF PAGES 81
14. MONITORING AGENCY NAME & ADDRESS (if different from Controlling Office) Office of Naval Research Arlington, VA	15. SECURITY CLASS. (of this report) UNCLASSIFIED
	15a. DECLASSIFICATION/DOWNGRADING SCHEDULE

16. DISTRIBUTION STATEMENT (of this Report)

Approved for public release: distribution UNLIMITED

17. DISTRIBUTION STATEMENT (of the abstract entered in Block 20, if different from Report)

UNLIMITED

18. SUPPLEMENTARY NOTES

19. KEY WORDS (Continue on reverse side if necessary and identify by block number)

ISAR, NCTR, Target Classification, Radar Image Recognition

20. ABSTRACT (Continue on reverse side if necessary and identify by block number)

In this investigation the Hughes Aircraft Company studied the use of structural, syntactic and statistical pattern recognition techniques for the automatic determination of target view in ISAR images of aircraft targets to be used in the automatic classification of these targets.

DD FORM 1 JAN 73 1473 EDITION OF 1 NOV 65 IS OBSOLETE

UNCLASSIFIED

SECURITY CLASSIFICATION OF THIS PAGE (When Data Entered)

CONTENTS

CONTENTS (Continued)

LIST OF ILLUSTRATIONS

LIST OF ILLUSTRATIONS (Continued)

LIST OF TABLES

FOREWORD

This report is a description of an investigation conducted by the Hughes Aircraft Company, Radar Systems Group, El Segundo, CA, to test the use of pattern recognition techniques for determining the target view in ISAR images of aircraft targets. Top and side view images of aircraft targets were used to test the techniques developed during this study. The tests included automatic view determination followed by classification using the method of moments.

The investigation was performed by the Signal Exploitation Programs Office of Hughes Radar Systems Group, for the Office of Naval Research, Arlington, VA, under Contract N00014-80-C-0940.

Dr. George A. Ioannidis served as the Hughes project manager. Commander Roger Nichols was the program manager for the Office of Naval Research, Arlington, VA.

This final report is submitted in accordance with the data requirements of Exhibit A, dated 25 September 1980, Sequence A002 of the Contract Data Requirements List 1423.

The authors acknowledge the support and contributions of Messrs. James Crosby, Manager, and Calvin Boerman, Assistant Manager of Signal Exploitation Programs at Hughes.

1.0 INTRODUCTION AND SUMMARY

This report contains the results of an ONR sponsored study by the Hughes Aircraft Company to determine the target view (top or side) presented by ISAR radar images of aircraft targets. The knowledge of target view is then utilized by algorithms for automatic target recognition, using the Method of Moments.

The aircraft radar images used in this investigation were generated by the application of the ISAR technique to turntable radar data and also data obtained from flying aircraft targets. The turntable data had been obtained at the RATSCAT facility under the AFAL E-3A Non-Cooperative Data Collection program and consist of X-band measurements against 1/3 scale models of an F-102, an F-5E, an A-10, an F-15 and a YF-16.

The stepped frequency technique was used to collect the data; 256 3.4 MHz frequency steps were used to synthesize an 870.4 MHz bandwidth. For the full scale targets, these measurements correspond to S-band data at 256 MHz bandwidth. The targets were placed on a rotary platform that rotated at 0.2 degree increments between adjacent bursts of the 256 frequency steps. Plan view images were obtained by positioning the target horizontally on the platform. Profiles were obtained by positioning the target vertically (the wings extending along the normal to the platform). In addition to the RATSCAT data, measurements on a flying DC-10, a 727, a 707 and an A-3 were used to form radar images. These data were obtained by an S-band radar operated by the Naval Ocean Systems Center (NOSC) in San Diego. By stepping the transmitter frequency pulse-to-pulse at 1.08 MHz increments over 256 pulses, this radar has an effective bandwidth of 276.5 MHz.

The aspects, resolutions and view of the images formed using the above data are given in Table 1. Examples of the best images from the above targets are shown in Figures 1 through 10.

During the study, algorithms (using structural, syntactic and statistical pattern recognition techniques) to determine the target view in ISAR images of aircraft were investigated. All the techniques were based on a

TABLE 1. RADAR IMAGES OF AIRCRAFT TARGETS GENERATED FOR THIS STUDY

Data	View	Number of Images per Target	Aspects	Resolution, meters
RATSCAT*	Plan	12	0.8-7°, 3.8-10°, 6.8-13°, . . . 33.8-40°	0.6
RATSCAT	Plan	12	140.8-147°, 143.8-150°, . . . 173.8-180°	0.6
RATSCAT	Profile	6	-180.0 to 173.8°, -177 to -170.8°, . . . -165 to -158.8°	0.6
RATSCAT	Profile	12	-21 to -14.8°, -18 to -11.8, . . . 12 to 16.2°	0.6
RATSCAT	Profile	6	158.8-165°, . . 161.8-168°, . . 173.8 to 180.0°	0.6
NOSC (DC-10)	Plan	10	Broadside	0.6
NOSC (DC-10)	Profile	9	Nose	0.6
NOSC (707)	Plan	12	Broadside	0.6
NOSC (707)	Profile	6	Nose	0.6
NOSC (727)	Plan	15	Broadside	0.6
NOSC (727)	Profile	3	Nose	0.6
NOSC (A3)	Plan	12	Broadside	0.6
NOSC (A3)	Profile	8	Nose	0.6
*RATSCAT Targets: F-102, F-5E, F-15, YF-16, A-10				

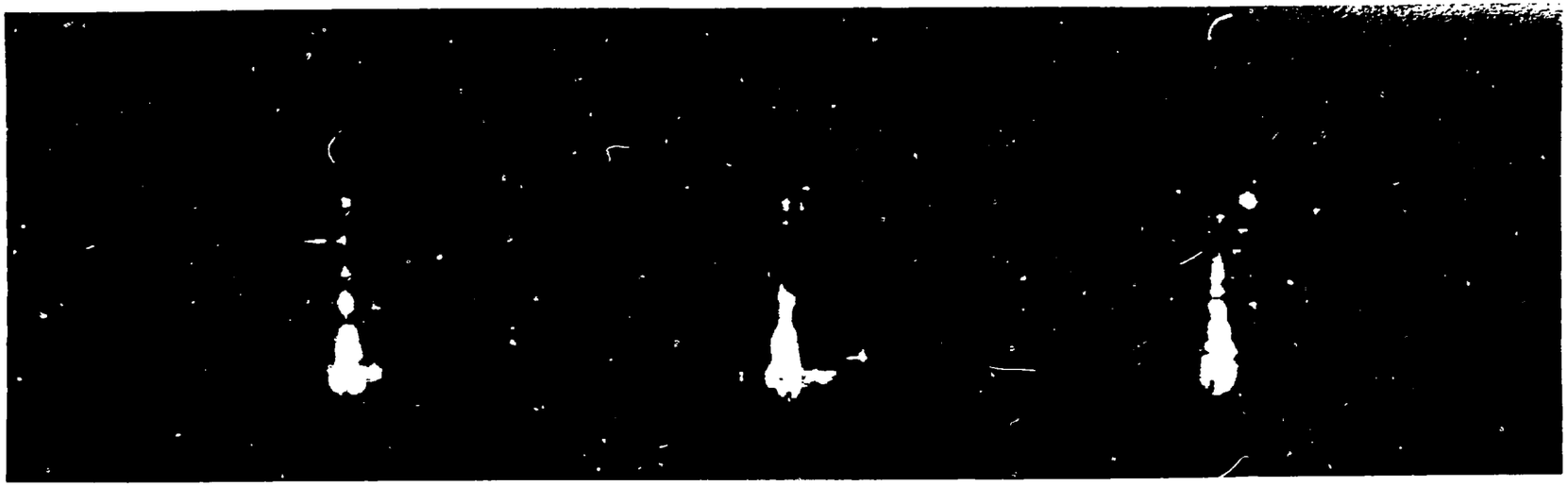

TAIL ASPECTS

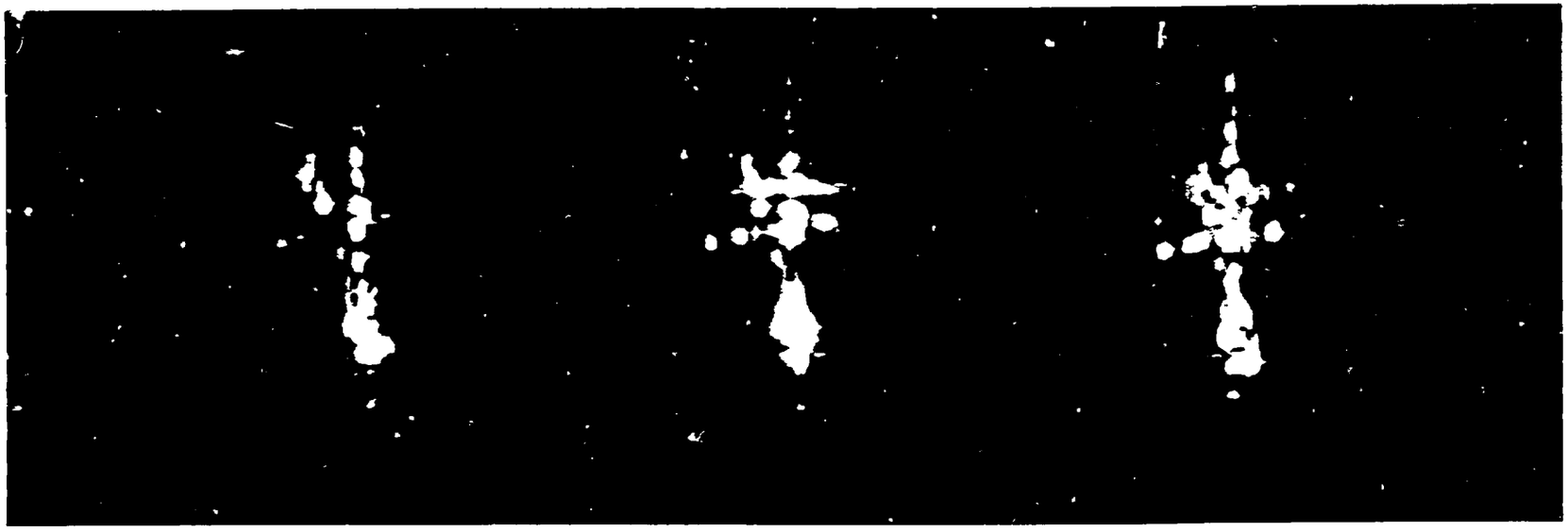

NOSE ASPECTS

Figure 1. Plan views of F-102 for 0.5 meter resolution

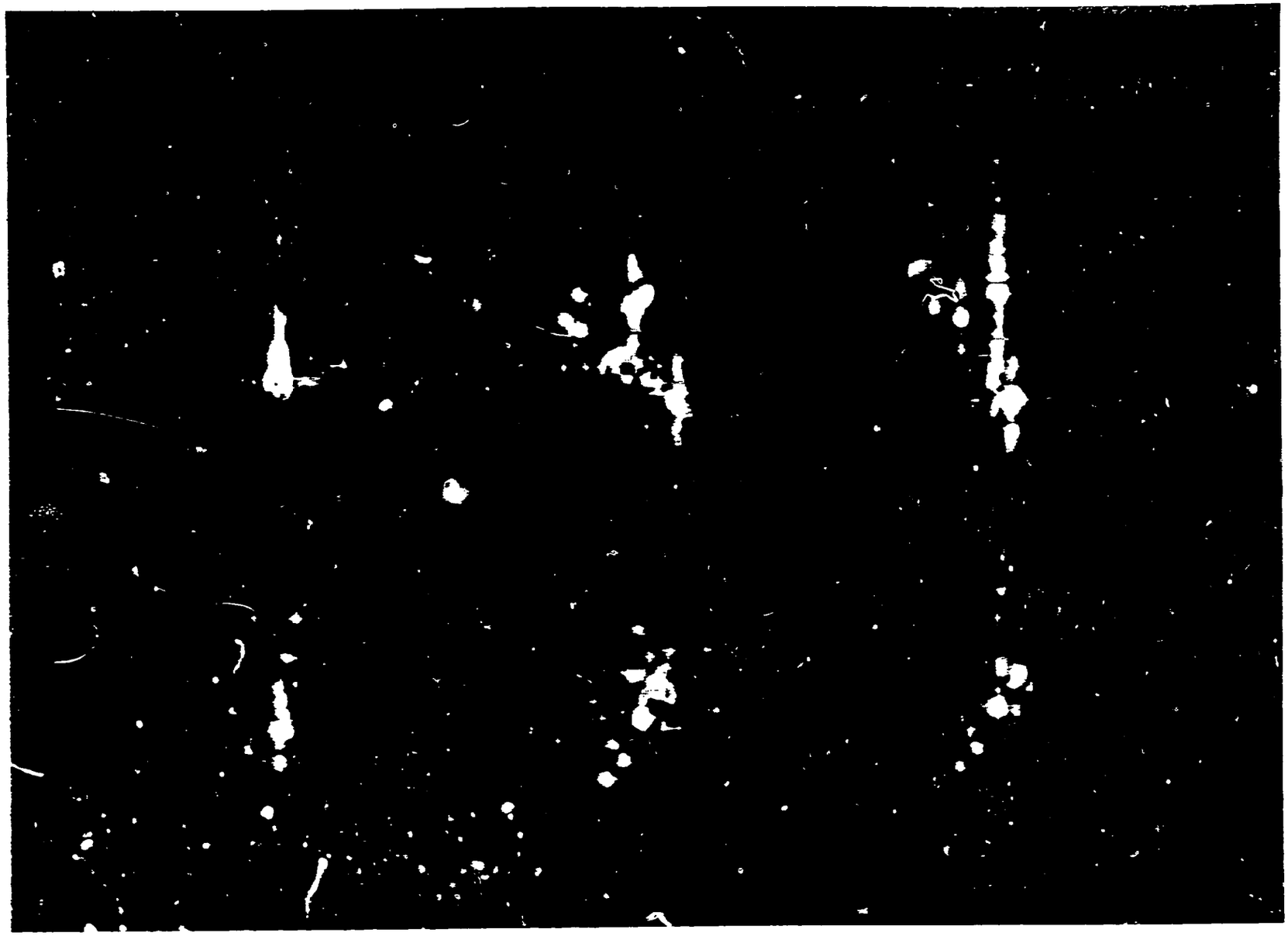

Figure 2. Plan views of F-102 tail aspect, F-15 40 degrees from the nose, F-16 10 degrees from the nose, F-5E tail, A-10 30 degrees from the nose, A-10 40 degrees from the nose (0.5 meter resolution).

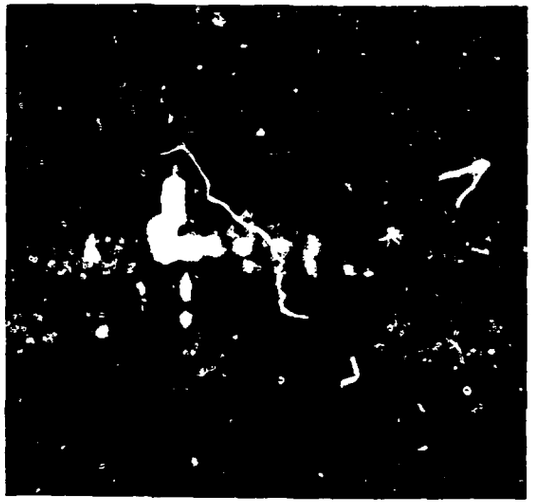

F-102 tail aspect

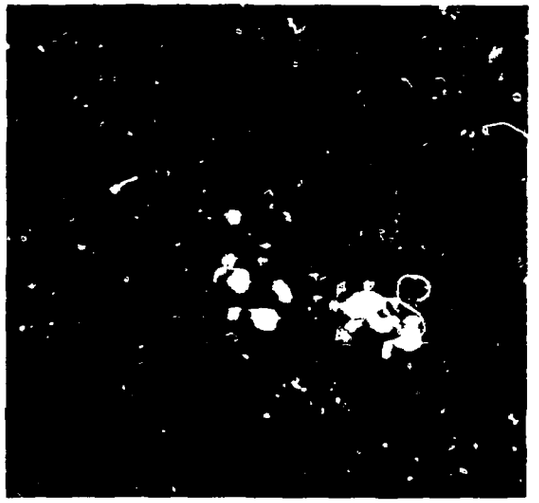

F-102 nose

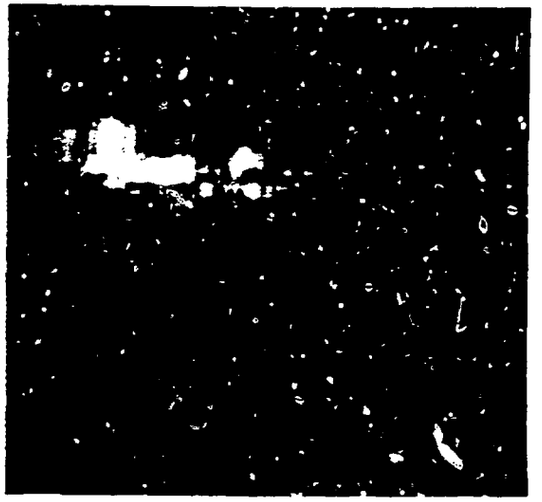

F-15 tail

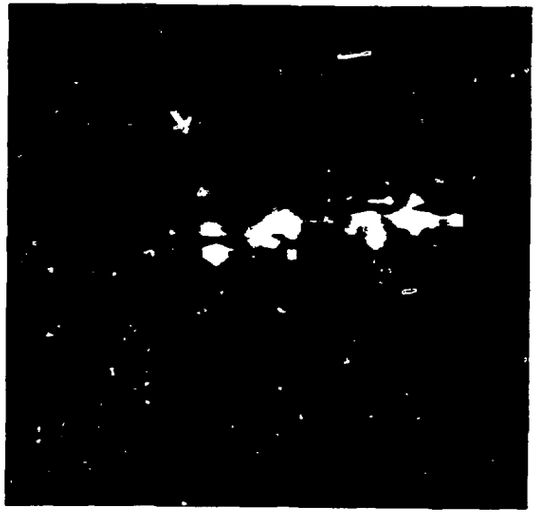

F-16 nose

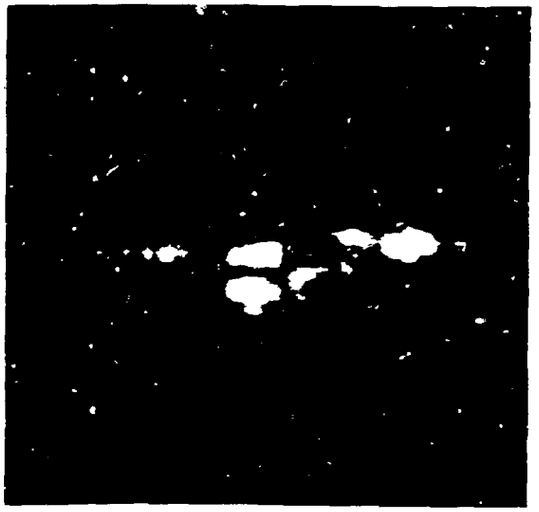

F-5E nose

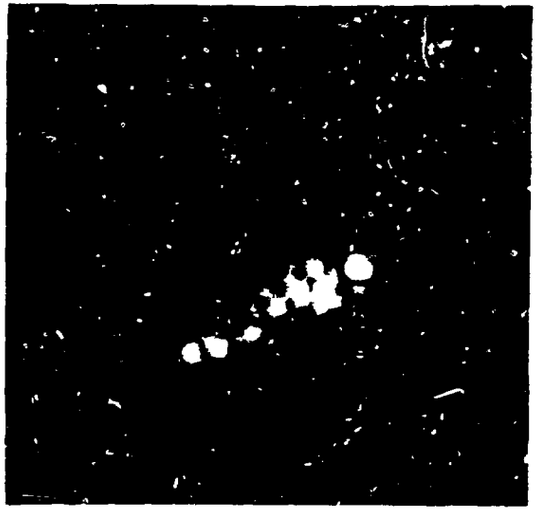

A-10 tail

Figure 3. Profiles of RATSCAT targets

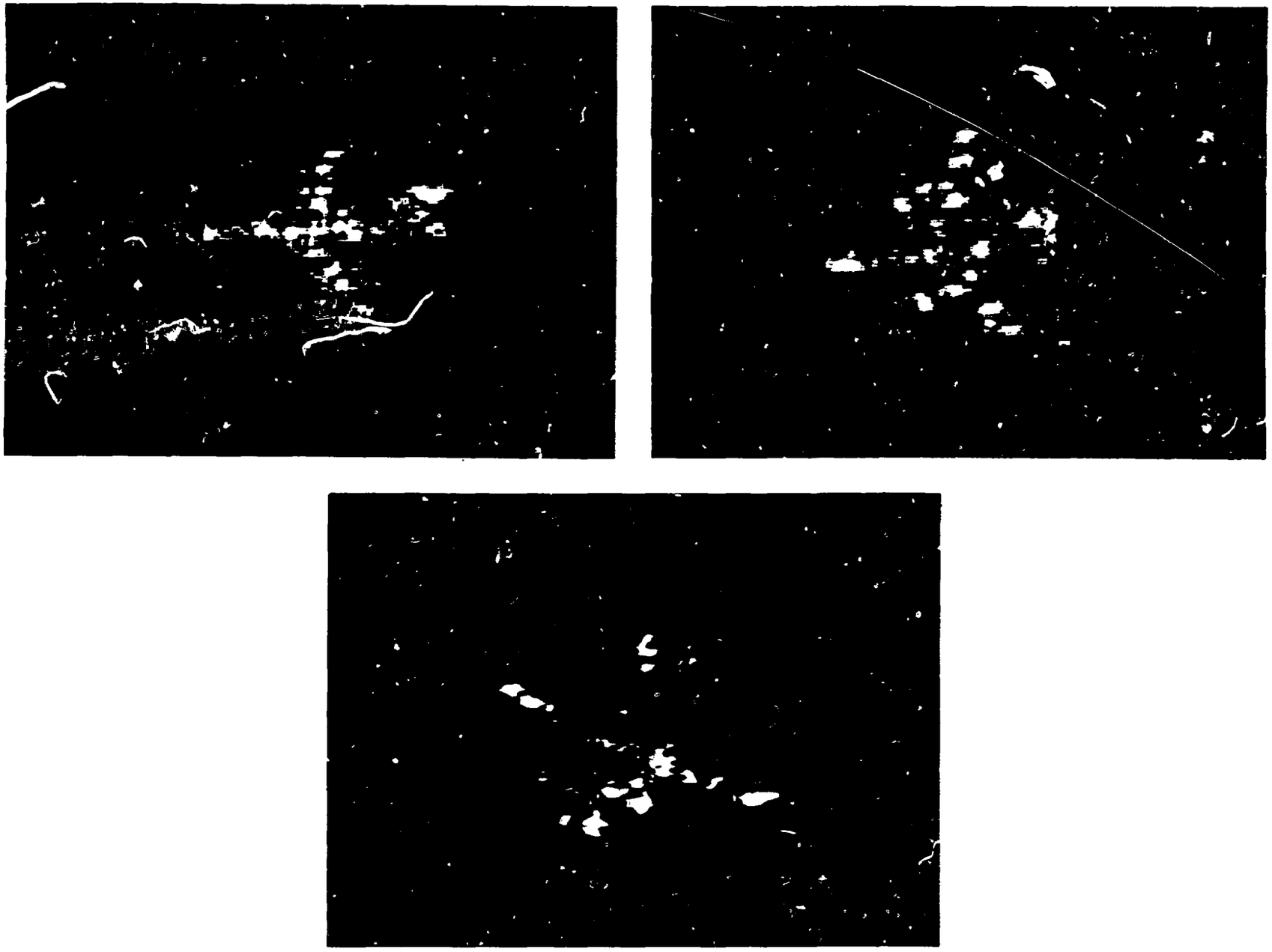

Figure 4. Plan views of a [illegible] a DC-10 and a 707

Figure 5. Plan views of a DC-10

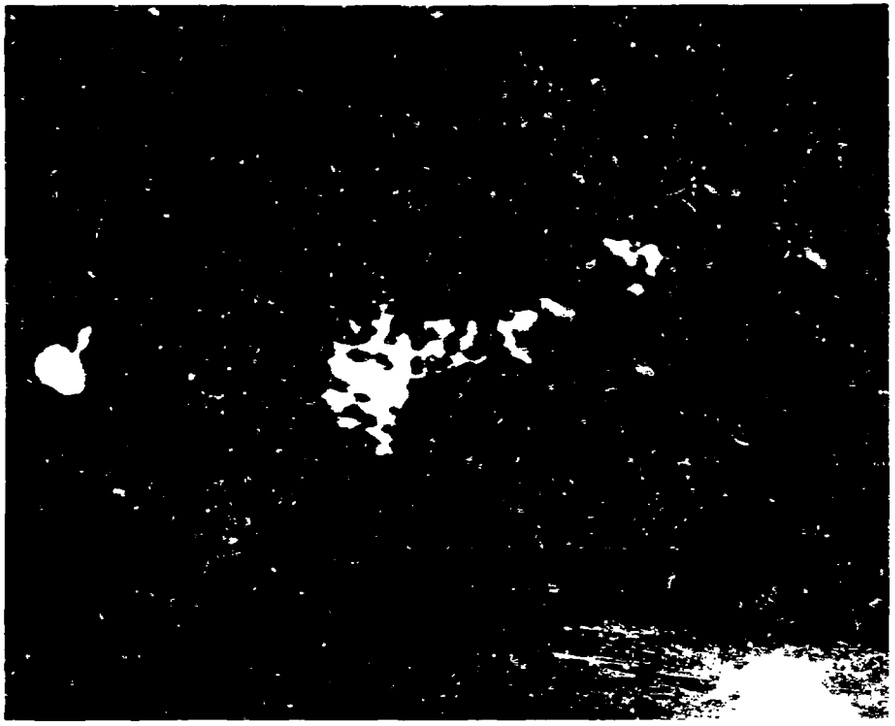

DC-10

F-5E

Figure 6. Profiles of DC-10 and F-5E

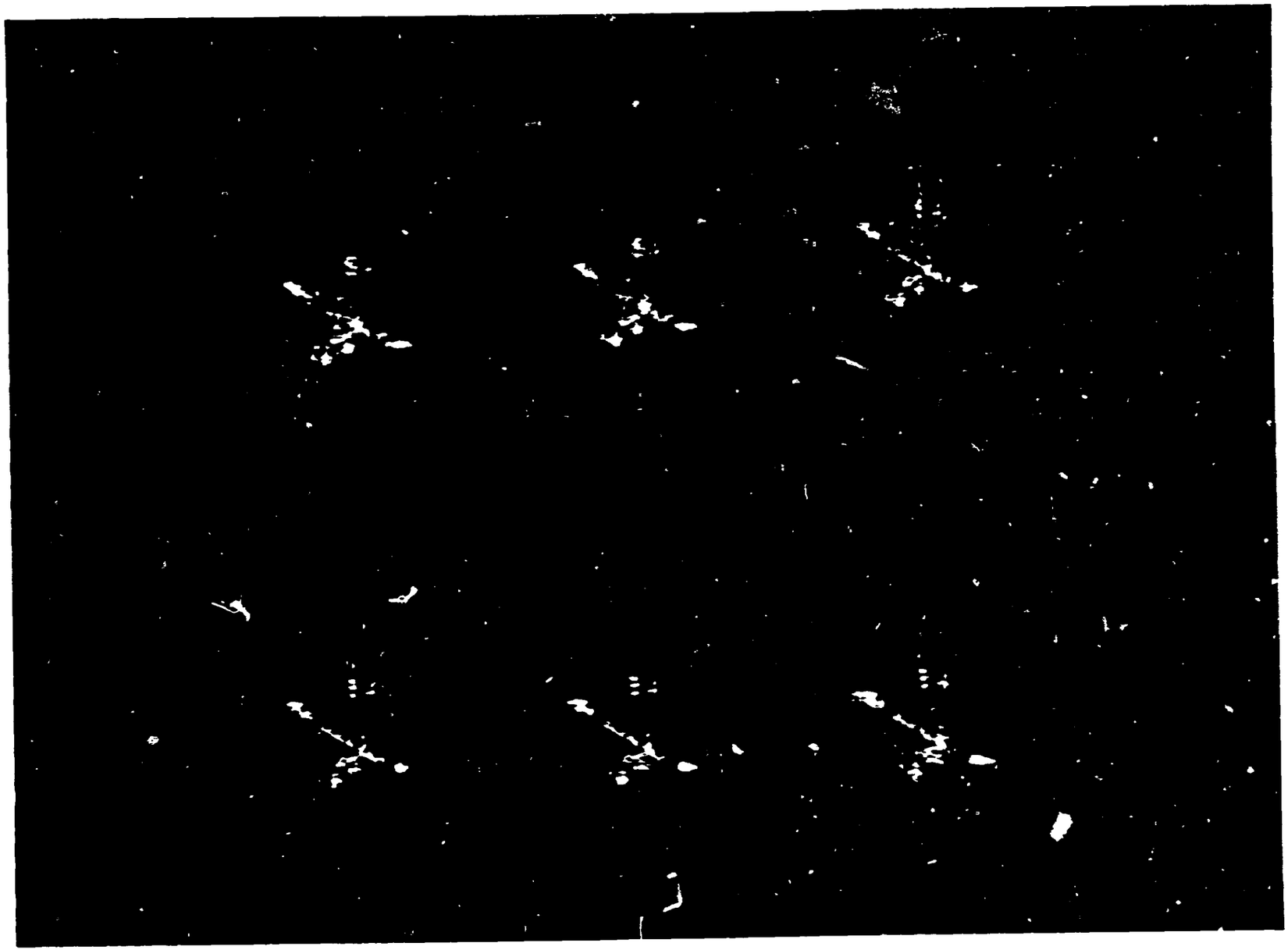

Figure 7 707 top views

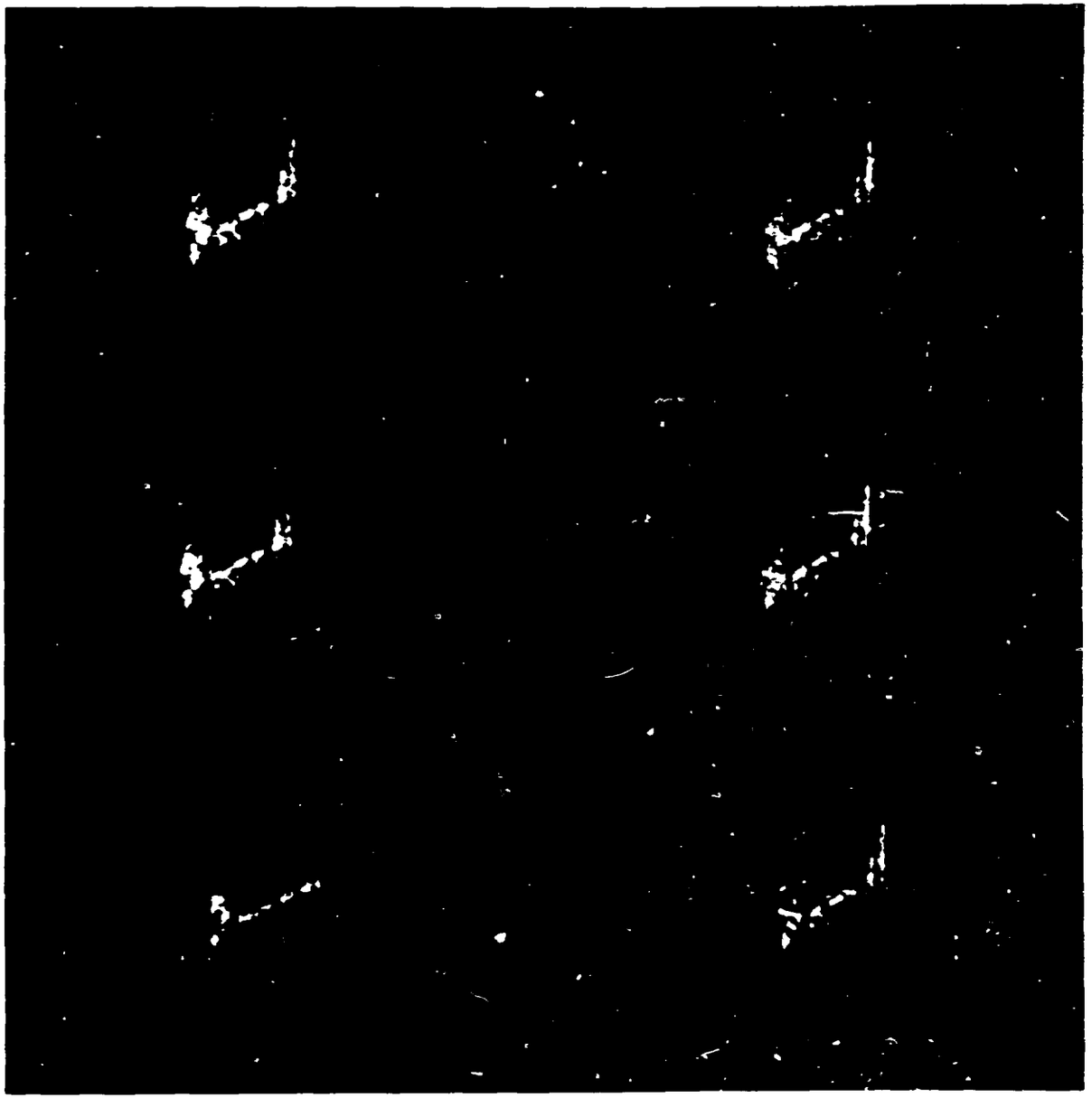

Figure 8. Profiles of 707

Figure 9. Top views and profiles of 727

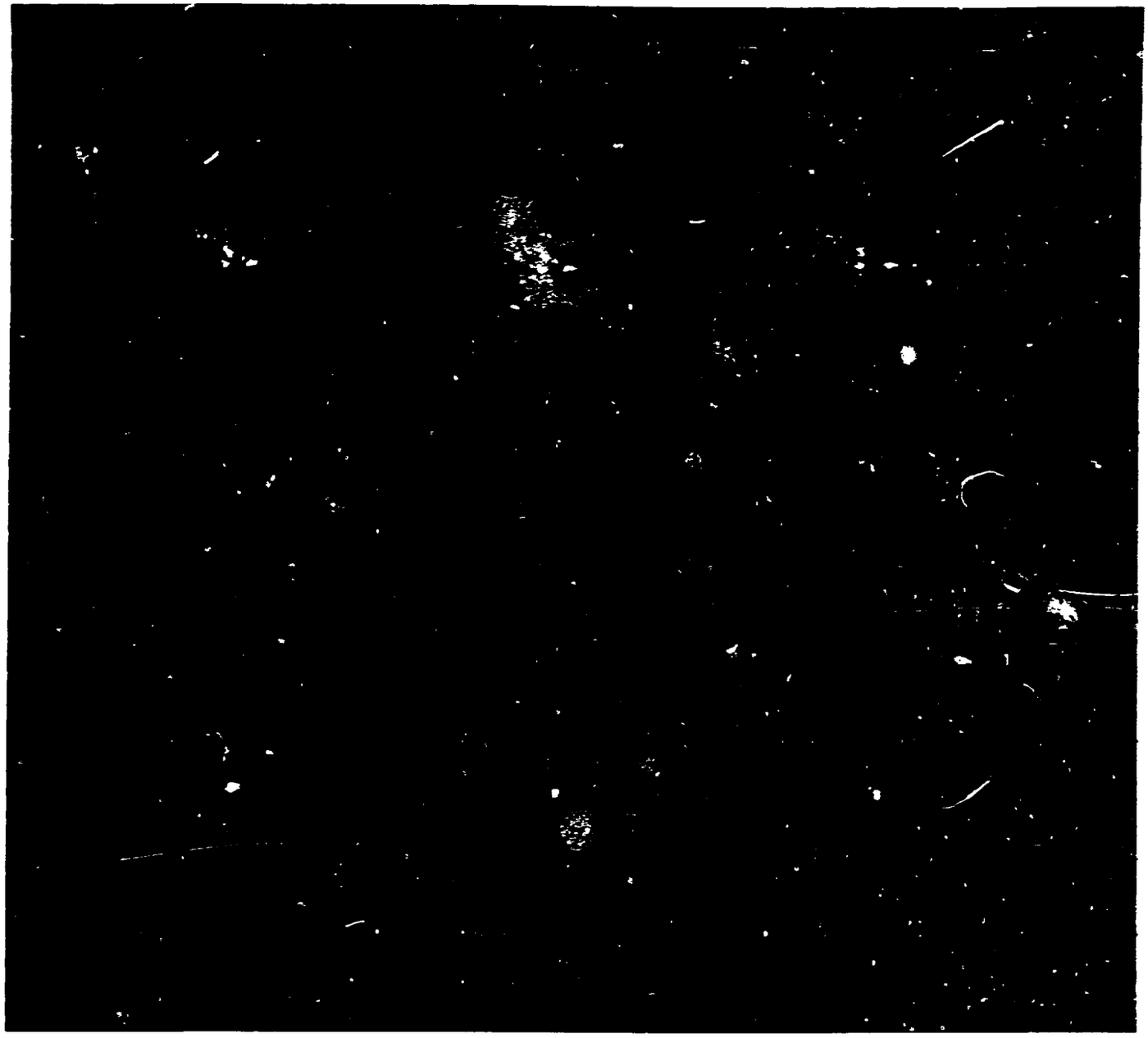

Figure 10. Top views and profiles of A3.

segmentation of the radar images using clustering. Since most radar images of aircraft targets consist of a collection of bright spots that correspond to strong scattering centers surrounded by low intensity regions, clustering tends to identify the location of the major scatterers.

In the syntactic schemes investigated, the cluster decomposition of radar images was used to construct a tree graph structure with clusters as nodes. These connected graphs or trees then were translated into strings of symbols that characterized the relative direction of a branch at a given node as described in detail in Section 4.0. An effort was made to identify the occurrence of symbols or symbol groupings that were characteristic of a view. For example, for a cross-like tree structure the symbol D was assigned to the node at the center of the cross. At the start of the investigation, it was thought that top views would result in such structures because of the wing extent. However, the profiles obtained using the RATSCAT data were often of very poor quality, and cross range sidelobes often produced a wing-like horizontal extent of the target similar to that observed on top views. Also as a result of the sidelobes, a horizontal branch at the location of the vertical stabilizer was often present in both top and side views. Since no unique distinguishing feature was identified when the RATSCAT targets were used, probabilities were assigned as to the occurrence of symbols and groups of symbols for each view. The relative position of symbols and the probability for a given grouping were described by a set of rules similar to the grammatical rules that describe the relative position of words in a sentence. Then a syntactic analysis was used to decide whether a given string of symbols satisfied the rules of the top or side view grammar. Since both grammars contained the same rules but with different probabilities assigned to their use, the syntactic analysis of the string resulted in a probability estimate for the class membership of the string. Then strings were classified according to the class with the highest probability. The best view determination results obtained with this technique were 75 percent correct. Using a similar technique on a few images of the DC-10, 727 and 707 from the NOSC data set, an 89 percent success rate was obtained.

During the investigation of syntactic classification schemes, an effort was made to identify parts of the image that tend to recur in one view or the

other. As a result of this effort, a technique that uses recurring regions of the image was developed. In this technique, top and side view composite images are formed from top and side views of similar targets in the training set. Then a distance measure is defined between an image and the composite. With this measure, images are classified by a nearest neighbor decision rule as top or side views. Tests using the RATCAT targets indicated that a 90 percent success rate could be achieved with this approach, which is described in Section 5.

A rule based structural approach to view determination was also investigated, and algorithms were developed to simulate a simple human-like interpretation of a radar image. This technique was tested using images of a DC-10, a 727 and a 707 from the NOSC radar data. A total of 54 images, 37 top views and 17 side views, were used to test the algorithm. The classifier gave the correct answer in 53 out of 54 cases; one side view of the DC-10 was classified as ambiguous.

Using the geometric moments (computed after cluster decomposition of the image), a Gaussian classifier was used to determine the view and classify the targets. The view determination performance of this statistical pattern recognition scheme applied to the RATSCAT targets was 78 percent correct for tail aspects and 85 percent correct for nose aspects. Target classification combined with view determination gave 71 percent correct classification for nose aspects and 80 percent correct for tail aspects for images classified as top views. For images classified as profiles, the corresponding results were 57 and 60 percent. A test was also performed to test classification without view determination using the RATSCAT targets. Classification was performed for a 10-class problem: F-102 top and side, F-15 top and side, F-16 top and side, F-5E top and side, A-10 top and side. The results were 44 percent correct for nose aspects and 38 percent correct for tail aspects.

These results indicate that for the RATSCAT targets, some common features do exist among the top views of all the targets that are different from similar features for side views. In general, the results of this investigation show that if the quality of radar images is good, view determination is possible and tends to improve classification.

Section 2 contains a summary of radar image classification using the method of moments. Radar image segmentation using clustering is discussed in Section 3. A syntactic approach to view determination is described in Section 4. Section 5 presents a view determination scheme using pattern matching. Section 6 is a discussion of a structural approach to view determination. Section 7 contains the statistical approach to view determination and classification using moments. Conclusions are given in Section 8.

2.0 RADAR IMAGE CLASSIFICATION USING THE METHOD OF MOMENTS

One of the more difficult problems in the design of a recognition system for pictorial patterns is the selection of a set of appropriate numerical attributes or features to be extracted from the object of interest for classification. The set of geometric moments of the image and invariant functions of these moments has been applied successfully to the recognition of optical pictures. [1], [2], [3] The geometric moments and invariant moment functions and their use in classifying radar images of targets are detailed in this section.

2.1 GEOMETRIC MOMENTS AND INVARIANT MOMENT FUNCTIONS OF IMAGES

The non central (p + q)th order moments of an NxM rectangular image field $f(x_i, y_j)$ are defined by

$$n_{pq} = \frac{1}{N \cdot M} \sum_{i=1}^{N} \sum_{j=1}^{M} f(x_i, y_j)\, x_i^p\, y_j^q \qquad (1)$$

where (x_i, y_j) are the coordinates of the (i, j) cell and $f(x_i, y_j)$ is the intensity function.

The central moments for the same rectangular image field are defined by

$$m_{pq} = \frac{1}{N \cdot M} \sum_{i=1}^{N} \sum_{j=1}^{M} f(x_i, y_j)\, (x_i - \bar{x})^p\, (y_j - \bar{y})^q \qquad (2)$$

where:

$$\bar{x} = \frac{n_{10}}{n_{00}} \qquad (3)$$

and

$$\bar{y} = \frac{n_{01}}{n_{00}} \tag{4}$$

The normalized central moments are defined by

$$\mu_{pq} = \frac{m_{pq}}{m_{00}},$$

and are invariant with respect to changes in the image intensity. Central moments as used in this discussion are the normalized central moments defined above.

From Equation (2), the central moments are invariant under translation but vary under rotations of the image. Using the theory of algebraic invariants, Hu [2] has shown that algebraic relations exist among the central moments of an image that are invariant under translation and rotation.

These invariant moment functions are of the form

$$\rho(m_{p_1q_1}, m_{p_2q_2}, \cdots m_{p_nq_n})$$

and are invariant under coordinate transformations. In particular, a set of invariants known as orthogonal invariants are functions whose value does not change under a rotation of coordinates, i.e., they are invariant with respect to the orthogonal transformation

$$\begin{pmatrix} x' \\ y' \end{pmatrix} = \begin{pmatrix} \cos\theta & \sin\theta \\ -\sin\theta & \cos\theta \end{pmatrix} \begin{pmatrix} x \\ y \end{pmatrix} \tag{5}$$

for any angle θ, i.e.,

$$(m'_{p_1q_1}, m'_{p_2q_2}, \cdots m'_{p_nq_n}) = (m_{p_1q_1}, \cdots m_{p_nq_n})$$

where the $m_{p_iq_i}$ are computed using the image intensity field f(x, y) and the $m'_{p_iq_i}$ are computed from f(x', y'). When these functions are invariant under rotations and/or reflections about one of the coordinate axes, they are called absolute orthogonal invariants. In this dicussion 'invariants' are these absolute orthogonal invariants.

Using the theory of algebraic invariants, Hu [2] has shown that the number of invariants involving moments from second to nth order (n = p + q) are the same as the number of moments with orders 2 to n, which is

$$N = \frac{(n + 4)(n - 1)}{2}$$

In optical and infrared image recognition systems, only invariant functions obtained from the second and third order moments are usually used. For these moments, the six absolute orthogonal invariants are given by

$$\rho_0 = (\mu_{20} + \mu_{02})^{1/2} = r \tag{6}$$

$$\rho_1 = \frac{1}{r^4}\left[(\mu_{20} - \mu_{02})^2 + 4\mu_{11}^2\right] \tag{7}$$

$$\rho_2 = \frac{1}{r^6}\left[(\mu_{30} - 3\mu_{12})^2 + (3\mu_{21} - \mu_{03})^2\right] \tag{8}$$

$$\rho_3 = \frac{1}{r^6}\left[(\mu_{30} + \mu_{12})^2 + (\mu_{21} + \mu_{03})^2\right] \tag{9}$$

$$\rho_4 = \frac{1}{r^{12}}\left[(\mu_{30}-3\mu_{12})(\mu_{30}+\mu_{12})\{(\mu_{30}+\mu_{12})^2-3(\mu_{21}+\mu_{03})^2\}\right.$$
$$\left.+(3\mu_{21}-\mu_{03})(\mu_{21}+\mu_{03})\{3(\mu_{30}+\mu_{12})^2-(\mu_{21}+\mu_{03})^2\}\right] \tag{10}$$

$$\rho_5 = \frac{1}{r^8}\left[(\mu_{20}-\mu_{02})\{(\mu_{30}+\mu_{12})^2 - (\mu_{21}+\mu_{03})^2\}\right.$$
$$\left. + 4\mu_{11}(\mu_{30}+\mu_{12})(\mu_{21}+\mu_{03})\right] \tag{11}$$

and one skew orthogonal invariant is given by

$$\rho_6 = \frac{1}{r^{12}}\left[(3\mu_{21}-\mu_{03})(\mu_{30}+\mu_{12})\{(\mu_{30}+\mu_{12})^2 - 3(\mu_{21}+\mu_{03})^2\}\right.$$
$$\left. -(\mu_{30}-3\mu_{12})(\mu_{21}+\mu_{03})\{3(\mu_{30}+\mu_{12})^2 - (\mu_{21}+\mu_{03})^2\}\right]. \tag{12}$$

Above ρ_1, ρ_2, ... ρ_6 have been normalized by powers of r to remove the effect of uniform scale changes. Because the quality of most radar images is not good compared to optical or FLIR images, the number of moments and invariants used in the classification of radar images [4] is much larger than six. In particular, all invariant functions involving central moments up to order n = 7 (i.e., a total of 33) were used in radar image classification tests performed in our earlier work in this area [4]. In these classification tests, all the above invariants as well as smaller subsets of these invariants were used to construct feature vectors. Classification results from these tests [4] are presented in Figure 11.

2.2 COMPUTATION OF TARGET ASPECT USING THE GEOMETRIC MOMENTS

If the rotationally invariant moment functions are used as features for classification, the target orientation in the image plane does not have to be computed. However, if that orientation is desired so that other recognition techniques, which need that information, can also be applied, the central moments can be used to give the target orientation as shown in Figure 12. Figure 12 also shows that if an ellipse is fit to the aircraft image, the orientation of the major axis, which usually coincides with the fuselage, can be obtained from (see Hu [3])

CLASSIFIER DECISION

TARGET PRESENT

	F102	F15	F16	F5E	A10	F111	UNKN
F102	14						4
F15		14	1				3
F16		1	13				4
F5E			1	10			7
A10					17		1
F111						7	2

PLAN VIEWS NOSE ASPECTS ONE METER RESOLUTION

CORRECT DECISION: 86
UNKNOWN: 21

Kth nearest neighbor classification results (1m resolution plan views) for K = 6 for 24 moments (best 12 from image and best 12 from edge detected image) normalized by their standard deviations for 0^{o} to 45^{o} aspects. Threshold for unknown = 0.5.

CLASSIFIER DECISION

TARGET PRESENT

	F102	F15	F16	F5E	A10	F111	UNKN
F102	13						5
F15		14	2				1
F16		4	7				7
F5E			1	10			7
A10					13		5
F111						4	5

CORRECTION DECISION: 90%
UNKOWN: 31%

Kth nearest neighbor classification results (1m resolution plan views) for K = 6 for 24 moments (best 12 from image and best 12 from edge detected image) normalized by their standard deviation for 45^{o} to 90^{o} aspects. Threshold for unknown = 0.5.

CLASSIFIER DECISION

TARGET PRESENT

	F102	F15	F16	F5E	A10	F111	UNKN
F102	13				2		3
F15		16					2
F16			16				2
F5E				11	2		5
A10	1				18		1
F111							

CORRECT DECISION: 94
UNKNOWN: 14

Kth nearest neighbor classification results (1m resolution plan views) for K = 6 for 24 moments (best 12 from image and best 12 from edge detected image) normalized by their standard deviations for 90^{o} to 135^{o} aspects. Threshold = 0.5.

CLASSIFIER DECISION

TARGET PRESENT

	F102	F15	F16	F5E	A10	F111	UNKN
F102	13						5
F15		14	2				2
F16	1	4	10	1			2
F5E	1	1	2	10			4
A10					17		1
F111							

PLAN VIEWS TAIL ASPECTS 1 METER RESOLUTION

CORRECT DECISION: 84
UNKNOWN: 15

Kth nearest neighbor classification results (1m resolution plan views) for K = 8 for 24 moments (best 12 from image and best 12 from edge detected image for 135^{o} to 180^{o} aspects. Threshold for unknown = 0.5.

Figure 11. Classification of plan views of aircraft radar images using moments.

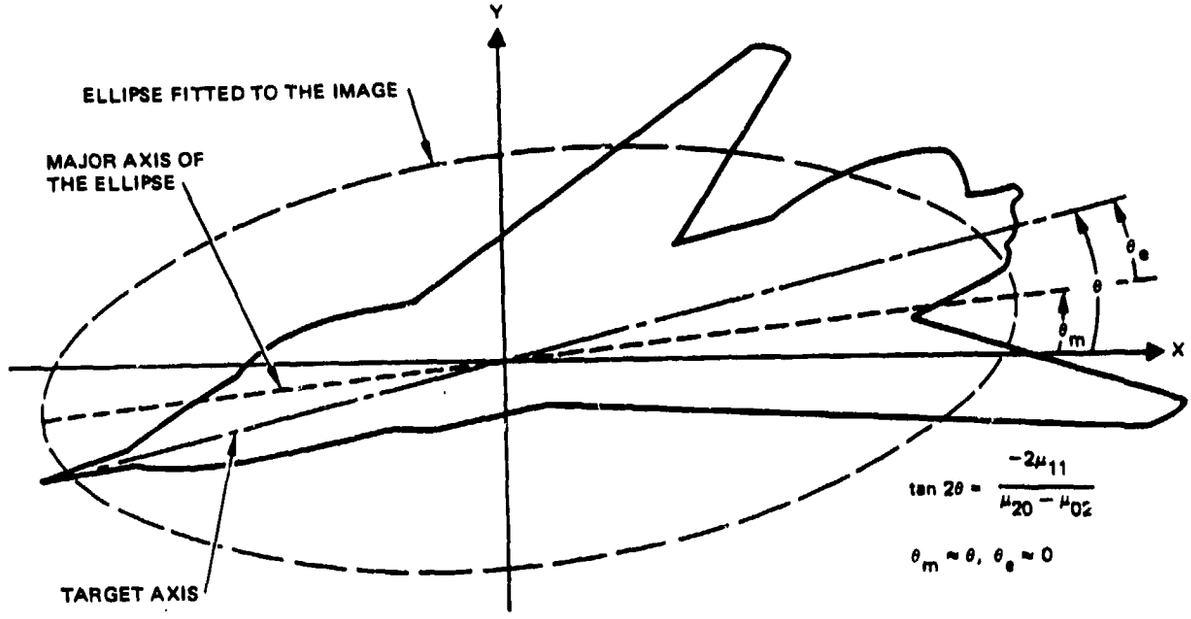

Figure 12. Computation of fuselage orientation by fitting ellipse to target image.

$$\tan 2\theta = \frac{-2\mu_{11}}{(\mu_{20} - \mu_{02})}, \tag{13}$$

where θ is the angle of this axis with the horizontal (x-axis).

In the previous Hughes study [4] the performance of the above formula in estimating the target aspect angle was tested by using the images of the five RATSCAT targets. The results are presented in Figure 13 in the form of a histogram that plots frequency of occurrence versus error in orientation angle estimate. A total of 36 images per target covering aspect angles from 0 degrees (nose on) to 180 degrees (tail) were used in constructing the plot in Figure 13.

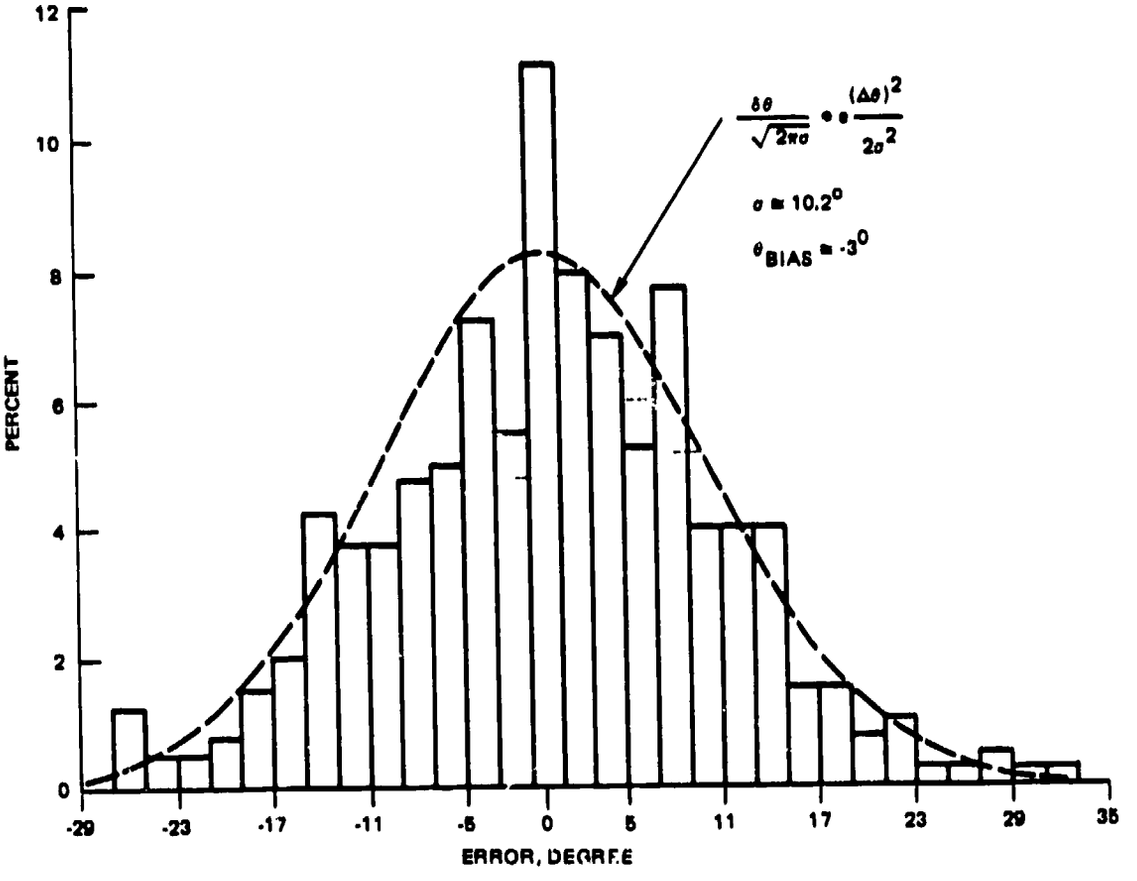

Figure 13. Aspect angle error distribution over all aspects for the five RATSCAT targets (plan views).

3.0 RADAR IMAGE SEGMENTATION USING CLUSTERING

Radar images of aircraft targets generally consist of a collection of bright spots surrounded by low intensity regions. The positions of these spots correspond to the locations of strong scatterers on the target. Thus a decomposition of radar images into segments consisting of groups of neighboring bright spots can be used to identify the major radar scatterers on an aircraft target. Such a decomposition can be obtained using the ISODATA clustering scheme developed by Ball and Hall [5, 6]. In outline form the essential steps of the algorithm are

1. Select initial center estimates.
2. Assign every sample to the cluster whose center is closest, using the current estimates of the centers.*
3. Compute new centers for each cluster and compute the "within-group variability" (i.e., the sum of the covariances of each component of the sample vectors for that group).
4. Split the average center of each group found in Step (2) into two centers if the within-group variability exceeds a threshold θ_E, which is set by the operator. The group is split by forming two new cluster centers from the original. The new centers are identical to the original, except for that component having highest variability, which is given the values $\bar{x} + \Delta$ and $\bar{x} - \Delta$ where $\bar{x}$ is the mean value for that component and Δ is some offset typically $\Delta = \sigma$. This results in the "birth" of a new cluster.
5. Regroup the samples using the new cluster points, and then again find the cluster centers for each group.
6. Compute inter-class distances between all pairs of cluster centers.
7. Combine groups whose distances apart are less than a threshold θ_c.
8. Iterate the procedure until no changes occur.

As seen from this brief description the ISODATA algorithm is a merging and splitting process which iterates over the image several times before coming up with the final set of clusters. In the original report [6] the assumption was made that if the algorithm was allowed to iterate enough times then it would converge to a stable set of clusters.

*The meaning of close depends on the data and the values of the parameters.

However, use of the algorithm on radar images of aircraft targets showed that the algorithm did not converge to a stable set of clusters. To improve the convergence properties of the algorithm, when used with radar images, considerable extensions were made during this study in such areas as finding optimal clusters of a 2-dimensional radar image and criteria for convergence of the clustering algorithm. In particular a criterion was introduced to determine when the merging and splitting process should be stopped and a new set of criteria was introduced to control which clusters should be split and which clusters should be merged. This revised version of ISODATA has better convergence properties when used on radar images and in the majority of cases tried during this investigation it correctly identified the major scattering centers on the target. In what follows there is a brief description of the criteria introduced to control the merging and splitting process of the ISODATA algorithm.

The criteria were derived from the scatter matrices used in multiple discriminant analysis. For each cluster the coordinates of the cluster center and the within-cluster scatter matrix were defined as follows

$$\bar{x}_k = \frac{M_{10}(k)}{M_{00}(k)} \tag{14}$$

$$\bar{y}_k = \frac{M_{01}(k)}{M_{00}(k)} \tag{15}$$

where $\bar{x}_k$ and $\bar{y}_k$ are the coordinates of the cluster center and

$$S_k = \begin{pmatrix} M_{20}(k) & M_{11}(k) \\ M_{11}(k) & M_{02}(k) \end{pmatrix} - \frac{1}{M_{00}(k)} \begin{pmatrix} M_{10}^2(k) & M_{10}(k)\,M_{01}(k) \\ M_{10}(k)\,M_{01}(k) & M_{01}^2(k) \end{pmatrix} \tag{16}$$

is the within-cluster scatter matrix

where:

$$M_{00}(k) = \sum_{i=1}^{N_k} \sqrt{A_i} \tag{17}$$

$$M_{10}(k) = \sum_{i=1}^{N_k} \sqrt{A_i}\, X_i \tag{18}$$

$$M_{01}(k) = \sum_{i=1}^{N_k} \sqrt{A_i}\, Y_i \tag{19}$$

$$M_{20}(k) = \sum_{i=1}^{N_k} \sqrt{A_i}\, X_i^2 \tag{20}$$

$$M_{02}(k) = \sum_{i=1}^{N_k} \sqrt{A_i}\, Y_i^2 \tag{21}$$

$$M_{11}(k) = \sum_{i=1}^{N_k} \sqrt{A_i}\, X_i\, Y_i \tag{22}$$

A_i is the intensity of the ith pixel in the kth cluster and N_k is the total number of pixels in the cluster.

Using the above, the total within cluster scatter matrix is defined by

$$S_W = \sum_{k=1}^{N_c} S_k \tag{23}$$

and the between clusters scatter matrix given by

$$S_B = \sum_{k=1}^{N_c} M_{00}(k) \begin{bmatrix} (\bar{x}_k - \bar{x}) \\ (\bar{y}_k - \bar{y}) \end{bmatrix} \left[(x_k - \bar{x}), (\bar{y}_k - \bar{y}) \right] \tag{24}$$

where N_c is the total number of clusters and $\bar{x}$ and $\bar{y}$ are the coordinates of the center of gravity of the entire data set defined by equations similar to Equations (14) and (15). Using the above definitions a clustering fidelity criterion is introduced (see also [7]) based on the ratio of between- to within-cluster scatter measures given by

$$J = tr(S_B)/tr(S_W), \tag{25}$$

where $tr(\cdot)$ indicates the trace (sum of the diagonal elements) of a matrix. Since,

$$tr(S_B) + tr(S_W) = tr(S_T) = \text{constant}$$

where S_T is the total scatter matrix of the data the fidelity criterion of Equation (25) can be modified to

$$(J+1) = \frac{tr(S_T)}{tr(S_W)} \tag{26}$$

This criterion was used to control the merging and splitting process of the ISODATA algorithm until the ratio of Equation (26) approached a predetermined value. Experimentation with aircraft radar images showed that J = 7 gave clusters which were consistently in agreement to those formed by human observers.

During execution of the algorithm $tr(S_W)$ was continuously updated using

$$tr(S_W) = \sum_{k=1}^{N_c} \left\{ M_{20}(k) + M_{02}(k) - \frac{M_{10}^2(k) + M_{01}^2(k)}{M_{00}(k)} \right\}$$

where N_c is the number of clusters. If clusters k_1 and k_2 are merged the resulting change in $tr(S_W)$ is given by

$$\Delta tr(S_W) = \frac{M_{10}^2(k_1) + M_{01}^2(k_1)}{M_{00}(k_1)} + \frac{M_{10}^2(k_2) + M_{01}^2(k_2)}{M_{00}(k_2)}$$

$$- \frac{\left(M_{10}(k_1) + M_{10}(k_2)\right)^2}{M_{00}(k_1) + M_{00}(k_2)} - \frac{\left(M_{01}(k_1) + M_{01}(k_2)\right)^2}{M_{00}(k_1) + M_{00}(k_2)} .$$

Using the above equations two clusters are merged if their centers are closer than a preset distance and if the value of

$$\left| tr(S_W) - \frac{tr(S_T)}{J+1} \right|$$

decreases as a result of merging.

The criterion for splitting clusters was based on the RMS extent of the cluster and on a prediction of the value of the ratio in Equation (26).

The predicted value of the ratio in Equation (26) was obtained using an estimate of the change in $tr(S_W)$ as a result of splitting given by

$$\Delta tr(S_W) = -d^2 \cdot M_{00}(k)$$

where

$$d = \frac{\text{RMS extent}}{2} .$$

The above criteria were used to control the merging and splitting process in ISODATA. The process stops when

$$\left| \operatorname{tr}(S_W) - \frac{\operatorname{tr}(S_T)}{J+1} \right|$$

is minimum.

Examples of cluster decomposition of aircraft radar images are shown in Figure 14.

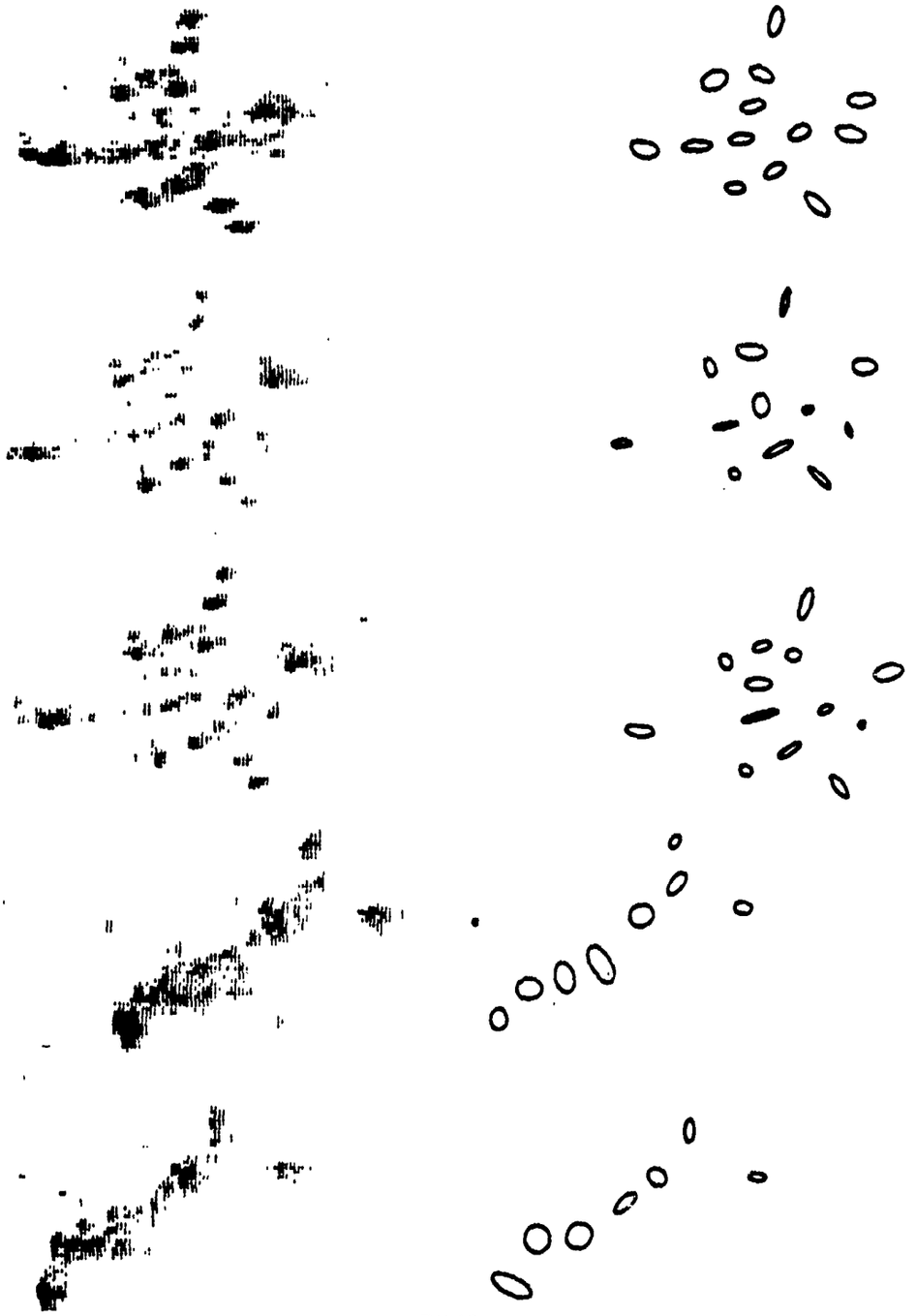

a. DC-10

Figure 14. Top and side view cluster decomposition.

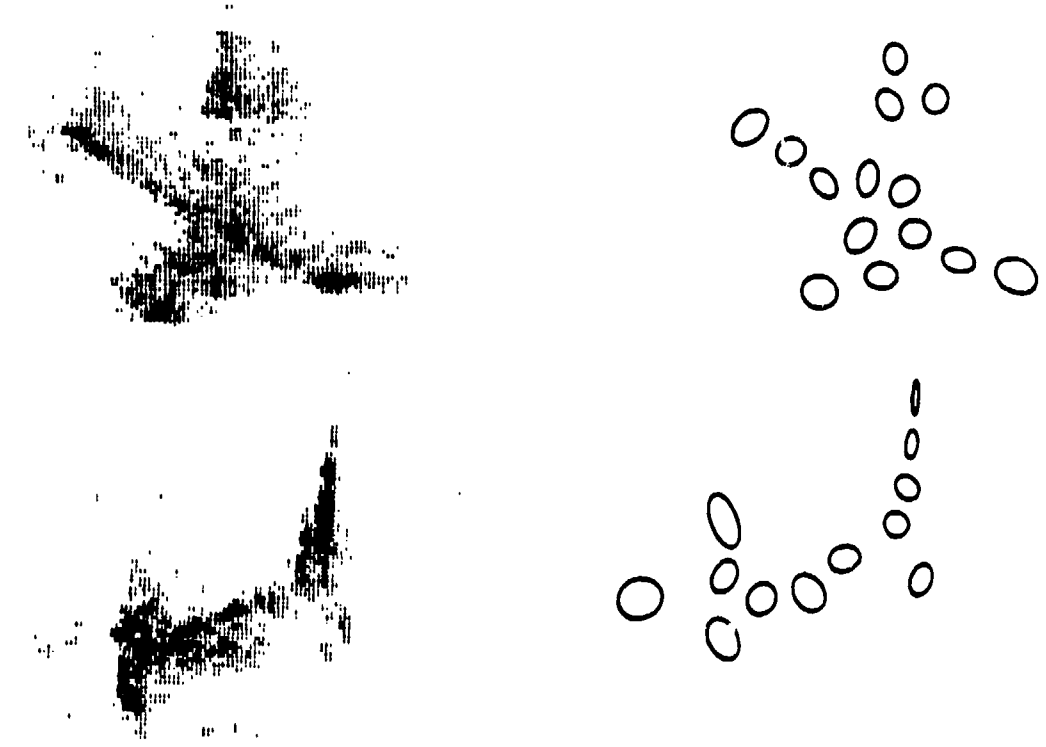

b. 707

c. 727

Figure 14. Top and side view cluster decomposition.

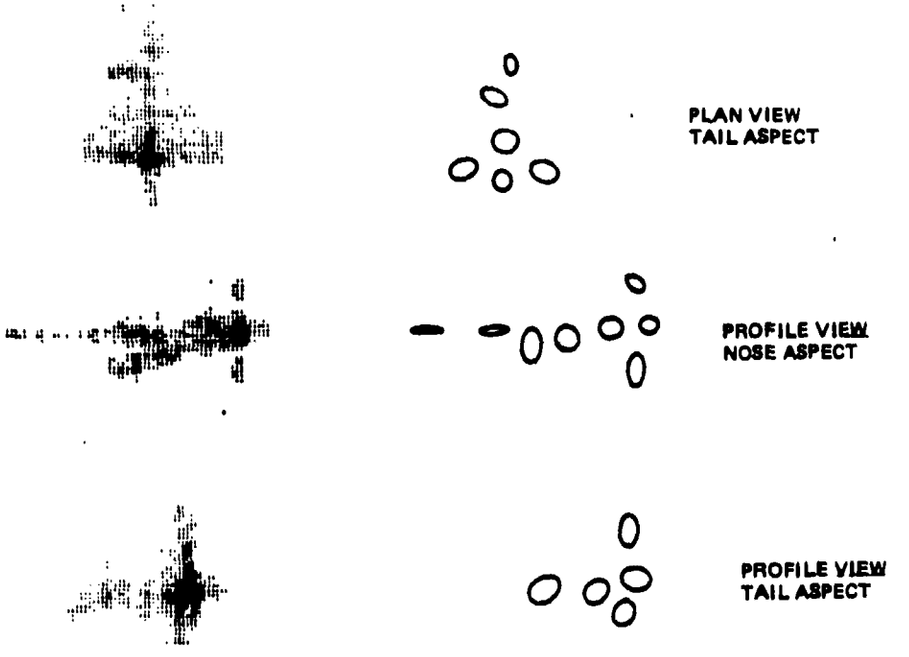

d. F-102

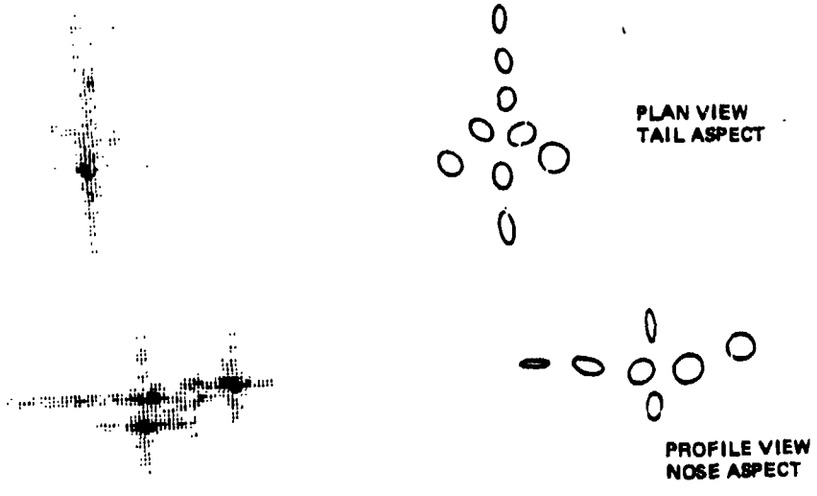

e. F-5E

Figure 14. Top and side view cluster decomposition.

4.0 A SYNTACTIC APPROACH TO VIEW DETERMINATION

It was anticipated that top views and side views could be distinguished by noting the prominent presence of wing-like structures on a top view, and of a tail-like structure on profiles. Furthermore, the presence of such structures should be easily determined from a simple graph representation of the given image, as follows:

The graph would consist of nodes which represent clusters of "bright points" in the image, obtained by ISODATA or by other clustering methods. Such clusters tend to represent the major scattering centers on the target. Some of the nodes are then connected by "edges" so as to form a graph. The graph is to be formed in such a way that a good prototypical top view would have two edges extending in opposite directions from a "main stem", forming a tree-graph in the shape of a cross. The two extending edges, supposedly representing wings, should indicate a top view. Such a cross structure lends itself to a simple syntactic representation.

With this kind of approach in mind, the images were processed, thresholded, and clustered, and a graph or tree was formed.

Two distinct sets of data were available for use: RATSCAT data, which provided a systematic set of top views and side views from known aspect angles, obtained from controlled rotation of each target on a rotary platform, and NOSC data, which provided data of the target in actual flight. The RATSCAT data provided image arrays with less detail and resolution than the NOSC data, and also appeared to be of poorer quality in general.

We will discuss the syntactic view determination work done with the RATSCAT data, and then with the NOSC data, noting that the work with NOSC data was more promising and therefore was developed further.

4.1 SYNTACTIC ANALYSIS OF RATSCAT IMAGES

For the RATSCAT images, the graph tree was formed by using the "minimal spanning tree" for the given nodes or clusters. Some alternative distance measures were used in forming the (minimal spanning) trees, and some spurious small clusters were removed in accordance with an adaptive threshold criterion.

These graphs or trees were then translated into strings, in a manner to be described later. From these strings of the top views, top view grammars were constructed, and from strings of profiles, side view or profile grammars were constructed. These grammars are then syntactic descriptions of their respective views.

A minimal spanning tree is defined as follows [see Meisel 8]:

A spanning tree of a connected graph G is a tree in G which contains every node of G. The weight of a tree is the sum of the weights of its edges. (Typically, the weight of an edge is its length, which is the distance between the nodes of the edge.)

A minimal spanning tree is the spanning tree of minimal weight.

In forming the minimal spanning trees, two alternative weight or distance measures were used. The first is the usual Euclidean distance metric

$$d = \sqrt{(\Delta x)^2 + (\Delta y)^2}$$

The second weight is based on the ratio of the between-cluster variance to the sum of the within-cluster variances and is given by

$$W_{ij} = \frac{M_{oo}(i)\, M_{oo}(j)}{M_{oo}(i) + M_{oo}(j)} * \frac{d^2}{M_{oo}(i)\, \sigma_i^2 + M_{oo}(j)\, \sigma_j^2}$$

where $M_{oo}(k)$ is the sum of the intensities of the pixels in the kth cluster, d^2 is the square of the distance between the two cluster centers and

$$\sigma_j^2 = \sigma_{x_j}^2 + \sigma_{y_j}^2$$

are the characteristic sizes (orthogonal variance components) of the jth cluster.

The transformation of tree to string was designed to yield a symbol D for a simplistic "wing-like" distribution of clusters, as illustrated by

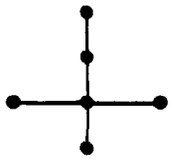

graph

C
C
D
C

string (CCDC)

The other two symbols, A and B, arise when the graph has an edge to only one side or the other of the "main" vertical path, e.g.,

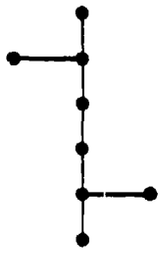

graph

C
A
C
C
B
C

string (CACCBC)

The C represents edges or segments of the main stem.

In an attempt to use the presence of D, and even the presence of an ACB or BCA which somehow "approximates" a D, as an indication of "wings" as seen on a top view, the first target (the F-102) was studied and revealed higher frequencies of D, ACB, and BCA in the side views. This occurred even after some editing of clusters in an attempt to remove spurious clusters which could mislead to the formation of a D as well as other symbols. We do not propose to use the mere presence of D, ACB, or BCA since the intuitive inclination is not supported by empirical indications.

In general, the top and side views of the RATSCAT targets, as processed to date, do not appear clearly distinguishable. Therefore we decided to try simple statistical grammars which use the frequency of

occurrence of each symbol in each position to distinguish the two views, and see what success rate can be obtained with these grammars.

The transformation of tree to string and the grammars used in the classification are

Transformation of Tree to String:

1. Select the vertically highest node
2. Subdivide the image plane into three angular sectors, as shown below, used in assigning symbols to branches of the tree graphs
3. Translate tree into string by making the following assignments, shown here for the single selected node:

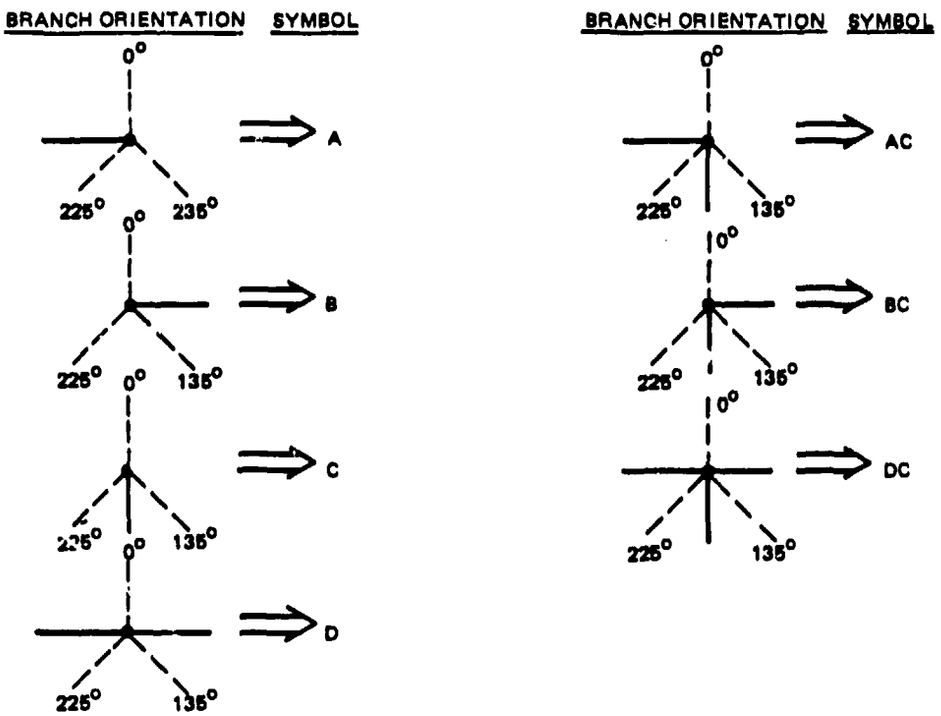

4. Select vertically lowest non-leaf direct descendant of current node, and remove this old current node and related vertices. If no such descendants, output the string and stop.
5. Go to 3.

The stochastic grammars studied here are of the following general form (for more details on graph grammars see the Appendix):

$X \longrightarrow Y_1 Y_2$

$X \longrightarrow UV_2$

$U \longrightarrow Y_1 Y_2$

$V_{i-1} \longrightarrow Y_i,\ Y_i V_i$
for $i = 3, 4 \ldots, n-2$

$V_{n-2} \longrightarrow Y_{n-1},\ Y_{n-1}\ Y_n$

$Y_i \longrightarrow P(A/i)^A$

$Y_i \longrightarrow P(B/i)^B$

$Y_i \longrightarrow P(C/i)^C$

$Y_i \longrightarrow P(D/i)^D$
for $i = 1, 2 \ldots, n$

X is the start symbol, and the nonterminal symbol Y_i is a position holder for the i'th position in the string.

$[Y_i \longrightarrow P(A/i)^A]$ means that the symbol A occurs in position i with probability P(A/i) (for the given view), and so on. The grammars differ only in these probabilities, which are readily estimated from the given sets of strings.

A preliminary attempt was made to find features which somewhat distinguish the top and side views for each target separately, i.e., which occur more frequently for one view than the other for a given target, and which repeat their preference in the several targets.

Each "feature" in this attempt was merely the presence of a given symbol in a specified position in the string derived from the image. Only two such features were found, and their bias or preference was deemed to be arbitrary.

Another suggested distinction between top and side views was that a top view would have basically one region of extensions from the main "stem" representing the fuselage, and a side view would have more than one (two--one for the wings and one for the tail).

This feature can be expressed on the strings in terms of having at least two non-C symbols separated by a string of Cs of length greater than zero, or perhaps greater than one. Several formal variations are possible for expressing this feature in terms of the strings. In any case, a quick study revealed this feature worked well for the F-102, but had a strong reversed (negative) correlation for the F-5E (the fourth target), so that it is not a consistent view-correlated feature.

4.1.1 Tests and Results

For the performance tests presented below the formation of the tree structure was subject to two parameters which determined the threshold for eliminating spurious clusters and selected the distance measure used in forming the minimal spanning tree. In the tables summarizing the results these two parameters are labeled FACTOR and IFUNC. The value of the parameter FACTOR is the percent of the average cluster intensity averaged over all the clusters and is used as the threshold for eliminating clusters. The value of the parameter IFUNC indicates the branch weight connecting two clusters which is used in the formation of the minimal spanning tree: IFUNC = 1 corresponds to the euclidean distance weight between the centers of the two clusters, while IFUNC = 2 corresponds to the weight based on the ratio of the between-cluster variance to the sum of the within-cluster variances for the two clusters.

For a given combination of the above two parameters the images were clustered and transformed into tree structures. The tree structures were then converted into strings of symbols as described above. By observing the resulting strings rules were derived to distinguish top and side view images. As described earlier these rules were based on the occurrence and position of the various symbols in the strings. The set of rules together with a set of probabilities to be applied to each view comprised the stochastic grammar used for the syntactic recognition of top and side view images. Stochastic top view and side view grammars, named GRAM 1, GRAM 2, ... GRAM 6 were derived from data obtained from 3 different choices of values for these parameters. The parameter values, view, and each grammar are related as indicated in Table 2.

TABLE 2. RELATION OF PARAMETER VALUES, TARGET VIEW, AND GRAMMAR NAME

	IFUNC = 1 FACTOR = 50	IFUNC = 2 FACTOR = 0	IFUNC = 2 FACTOR = 50
Top View	GRAM 1	GRAM 3	GRAM 5
Side View	GRAM 2	GRAM 4	GRAM 6

In addition, two non-stochastic grammars were formed:

GRAM 7 -determines presence of a D, and

GRAM 8 -determines presence of two regions of A or B or D separated by at least 2 C's.

The stochastic grammars GRAM 1 through GRAM 6 were tested on the data from which they were formed. The non-stochastic grammars GRAM 7 and GRAM 8 were not formed from any data, and were tested on the strings produced with IFUNC = 2 and FACTOR = 50.

Given a string and a grammar (GRAM), the computer algorithm determines whether the string can be in the grammar at all (i.e., parses the string) and if so, computes a value which ordinarily represents the probability of the most probable derivation, but which can be used as a "measure of membership" in the set represented by the grammar. The view of a given string is determined by selecting the grammar for which the above described measure is higher.

Three such tests were performed, one using GRAM 1 and GRAM 2 with the data from which they were formed, the second using GRAM 3 and GRAM 4, and the third with GRAM 5 and GRAM 6.

Finally, measures were obtained for membership in the sets represented by GRAM 7 and GRAM 8 for strings produced with IFUNC = 2, FACTOR = 50. All the above tests were performed on strings obtained from the first four RATSCAT targets F-102, F-15, F-16, and F-5E using six tail aspect and six nose aspect images per target for the top views, and 12 nose and 12 tail for the profiles.

The results were

FOR GRAM 1 AND GRAM 2

		Determined view	
		Top	Side
Actual view	Top	36	12
	Side	23	73
Overall = 75.5 percent correct			

FOR GRAM 3 AND GRAM 4

		Top	Side
	Top	28	20
	Side	32	64
Overall = 64 percent correct			

FOR GRAM 5 AND GRAM 6

		Top	Side
	Top	34	14
	Side	26	70
Overall = 72 percent correct			

As for the two nonstochastic grammars GRAM 7 and GRAM 8 mentioned earlier, no significant correlation with or implication regarding target view was noticed for either grammar individually, or in combination.

4.2 SYNTACTIC ANALYSIS OF NOSC DATA

Since a syntactic description typically intends to describe "structure," specifically spacial structure, images which had no discernible ("humanly recognizable") structure were not used. Furthermore, since the NOSC data are real flight data, each image is not strictly a pure top view or side view, so that the view (as either a top or side view) of many images could not be determined by any means. Some good images were obtained which seemed amenable to syntactic analysis, and only these selected images were used.

The approach used for the RATSCAT data served as a starting point; modifications to the graph forming algorithm were developed to make top views conform, as much as possible, to a generic graph such as the one in Figure 15, without unduly forcing the side views to conform to the top-view model graph.

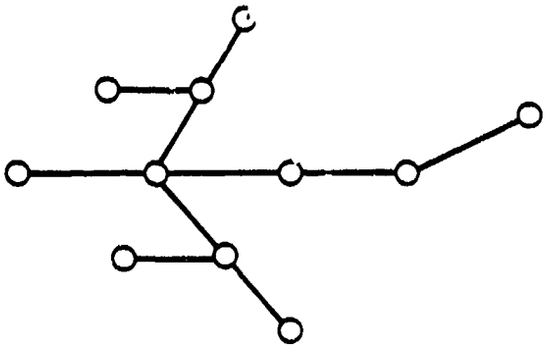

Figure 15. Ideal top-view graph.

The graph forming is based on the minimal spanning tree algorithm, and the primary modifications involve incorporation of cluster orientation into the distance measure used in that algorithm. Furthermore, this version of the minimal spanning tree algorithm was made applicable to portions of the tree, leaving previously formed portions intact.

The result of applying this modified algorithm, as compared with forming a simple minimal spanning tree, is illustrated in Figure 16, using top views of a DC-10 and a 727. Graphs formed by this algorithm are also illustrated in Figure 17.

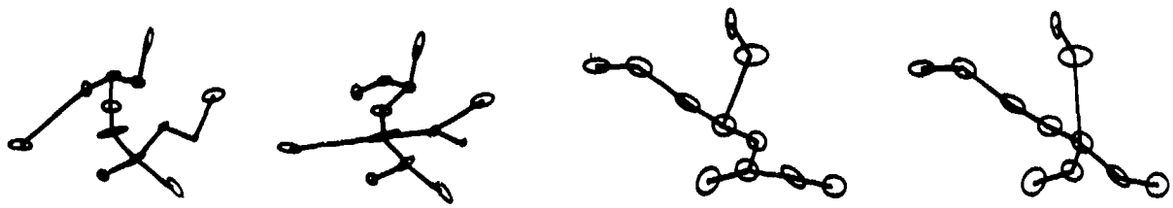

a. DC-10 b. 707

Figure 16. Results of pure minimal spanning tree algorithm (left) and final modified algorithm (right).

The purpose of including orientation is to force the tree to connect nodes in straighter lines. For example, assuming the orientation of the plane is known (from the flight trajectory), emphasizing this orientation in the distance measure tends to connect the clusters along the fuselage in the resulting tree.

Clusters presumably representing wings were determined by selecting two "wing-tip" nodes – i.e., the nodes of greatest distance from the presumed fuselage, one on each side of the fuselage, finding the path (in the tree graph) from each of these to the fuselage, determining the "orientation" of each wing by computing a line of least squares fit for each wing, and using the orientation of this line in reforming the section of the graph tree representing the respective wing. This process results in connecting the clusters in a straight or smoother line along each wing.

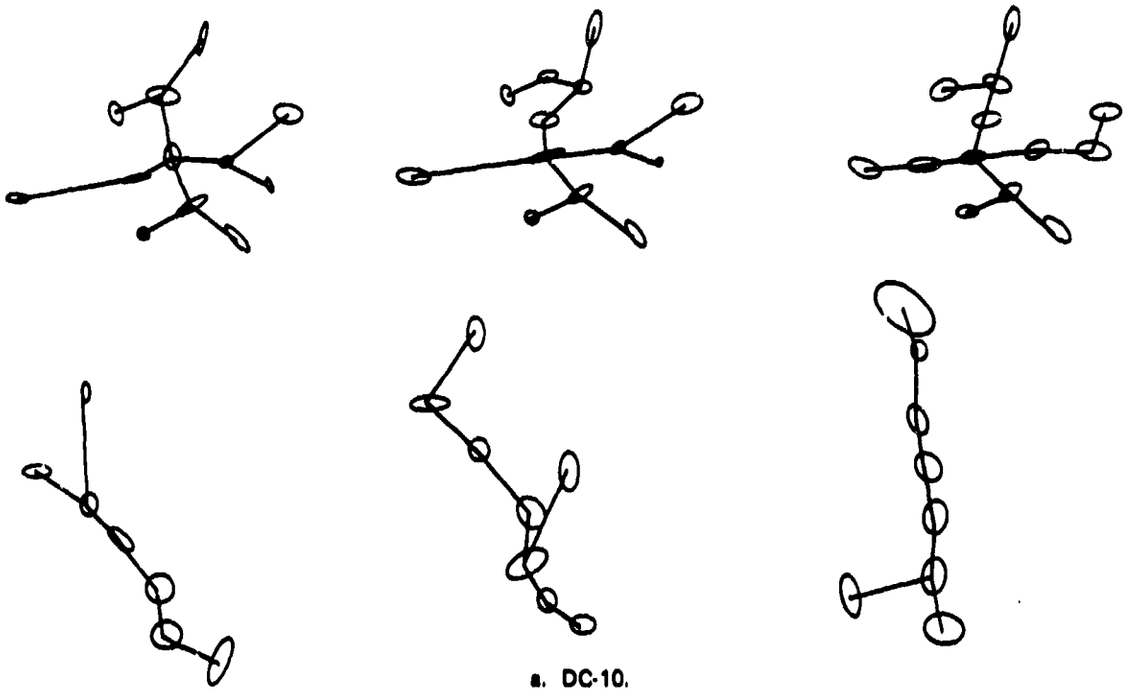

a. DC-10.

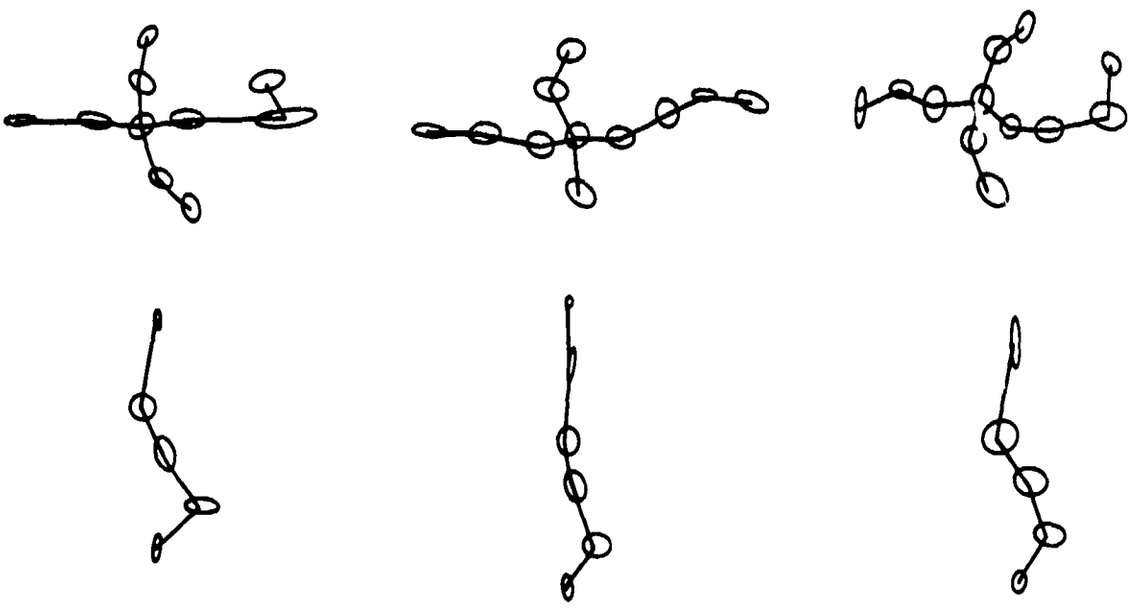

b. 727

Figure 17. Graphs formed from top views (top) and side views (bottom).

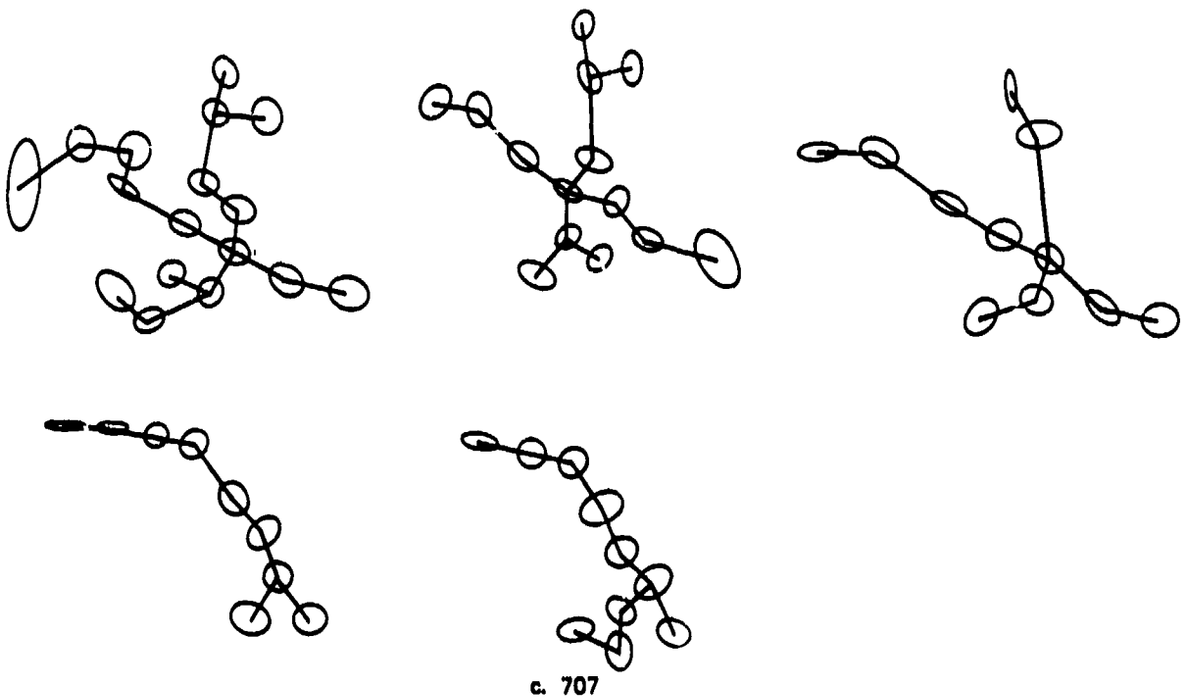

c. 707

Figure 17. Graphs formed from top views (top) and side views (bottom).

As with the RATSCAT data, the same idea of using protrusions to either or both sides of a main path is used in translating the graph to a string. However, the description of these protrusions (particularly in regard to which side of the main path the protrusion extends) has been refined to accommodate cases where nodes on the main path do not line up in a sufficiently straight line.

For these data, simply using the presence of a D (i.e., symbol representing a "cross," or a protrusion extending to both sides of the main path) to indicate a top view yielded 89 percent success (for the selected NOSC images).

The successes and failures for each of the three targets are given in Table 3.

TABLE 3. NUMBER OF SUCCESSES AND FAILURES OF THE VIEW DETERMINATION FOR EACH VIEW

Presented View		Determined View: Top	Determined View: Side
	Top	10	0
	Side	1	8

a) DC-10

Presented View		Determined View: Top	Determined View: Side
	Top	15	0
	Side	0	3

b) 727

Presented View		Determined View: Top	Determined View: Side
	Top	11	1
	Side	4	2

c) 707

Overall Correct = 89 percent

5.0 AIRCRAFT VIEW DETERMINATION BY MATCHING WITH "COMMON REGIONS"

In proposing a syntactic approach to view determination, it was suggested that the grammars for each view could be constructed by using recurring substructures - i.e., parts of the images which tend to recur in one view or the other. In this section such recurring regions of the images are used. However, the most successful "grammar" constructed with these is trivial with respect to grammatical structure, and the method presented here is more simply described without references to any grammatical constructs.

The test results for the method proposed here indicate that approximately 90 percent success can be achieved with some confidence.

5.1 ALGORITHM DESCRIPTION AND RESULTS

5.1.1 The Basic Procedure

1. Hard Limit each image from continuous grey level to ±1 (+1 if intensity is larger than the threshold and -1 if it is less).
2. "Smooth" the image (i.e., pass through a low pass filter).
3. Form a composite image for each group of similar targets using images over several aspect angles for each view.
4. Compute similarity measure between each composite and each image.
5. Normalize each similarity measure to a given composite by the maximum measure obtained for that composite in the training set.
6. Determine target view in testing set according to a "nearest neighbor" criteria (i.e., assign the target view of the most similar composite).

5.1.2 Forming the Composite Image

A composite image of a set of images is formed by arithmetic addition of the images, followed by some hard limiting on the absolute values. For example, for two image arrays A and B normalized so that

$$-1 \leq A(i,j) \leq 1$$

and

$$-1 \leq B(i,j) \leq 1$$

a composite C is formed by

$$D(i,j) = A(i,j) + B(i,j)$$

$$C(i,j) = \frac{D(i,j)}{|D(i,j)|} U_T(|D(i,j)|)$$

where: U_T is a step function defined by

$$U_T(x) = \begin{cases} 1 & \text{for } x \geq T \\ 0 & \text{otherwise} \end{cases}$$

for some selected threshold T. The hard limiting recovers an image more similar in type to the images from which the composite was formed as shown in the example below:

Example:

1	1	1	-1	-1	1	1	-1	1st image
1	1	-1	1	-1	-1	1	1	2nd image
1	1	-1	-1	-1	-1	1	-1	3rd image
3	3	-1	-1	-3	-1	3	-1	Sum
1	1	0	0	-1	0	1	0	Composite

This composite was formed by hard limiting the absolute values of the sum array, using a threshold of 3.

In this simple binary case, the composite represents the "points" or "positions" which are in agreement or in common to the three images; it is simply an "intersection" or "common region" of the three images.

By varying the threshold, different composites can be obtained. For a threshold ≤1, the composite represents a type of hard limited "average" image.

A composite of top views of the F-102, F-15, F-16 and F-5E for tail aspects, and a composite of side views of the same targets are illustrated in Figure 18. These composites were formed using a generalized form of hard limiting, as discussed below.

Figure 18. Composites for tail aspects from images of F-102, F-15, F-16 and F-5E aircraft.

5.1.3 Generalized Hard Limiting

The images from which the composites are formed can be binary (±1), but if any significant smoothing is done, they also have a variety of grey levels between -1 and 1. Therefore the hard limiting is generalized to recover an image of this type.

The generalized hard limiting is based on a powered sine function, as illustrated in Figure 19:

$$\text{Let } P(x) = \left[\sin^{C}\left[(x-T)\frac{\pi}{2T}\right]+1\right]/2 \qquad \text{for } 0 < x < 2T.$$

As c approaches 0, this function approaches hard limiting (i.e., a step function). The generalized hard limiting on the absolute values in an array A(i, j) is given by

$$C(i,j) = \frac{A(i,j)}{|A(i,j)|} P(|A(i,j)|)$$

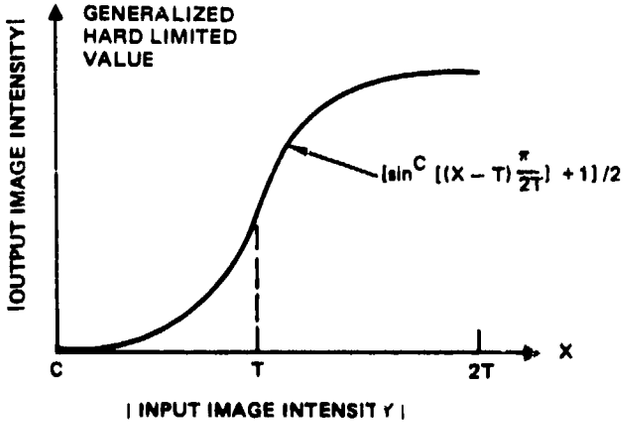

Figure 19. Generalized hard-limiting function. (C=1 is illustrated. As C approaches O, this function as computed in the program RECOV approaches hard-limitting; As C increases, a linear function is approached.)

5.1.4 The Similarity Measure

The basic measure of similarity between images is the "size" or extent of their "intersection" or common region. Specifically, it is the sum of the absolute values in their composite.

If we define the generalized hard limiting function G by

$$G(x) = \frac{x}{|x|}P(|x|)$$

(where P is as defined previously), then the similarity between two image arrays A and B is given by

$$\sum_{\text{all } i,j} |C(i,j)|$$

where:

$$C(i,j) = G(A(i,j) + B(i,j)).$$

However, the similarity measures computed in the basic procedure, between an image and a composite, are normalized by the "size" of the composite, where the "size" of an image A(i,j) is given by

$$\sum_{\text{all } i,j} |A(i,j)|$$

Therefore the similarity between an image B and a composite A was computed as

$$\frac{\sum |C(i,j)|}{\sum |A(i,j)|}$$

where:

$$C(i,j) = G(A(i,j) + B(i,j))$$

To compensate for a possible bias toward one view or another, a bias factor F is introduced, and each similarity computed between an image and a top-view composite is then multiplied by F, and the product is presented as the adjusted similarity value. Thus F > 1 favors a determination of top view, F < 1 favors a side view determination, and F = 1 is neutral.

$$\text{Adjusted similarity} = \begin{cases} \text{similarity} * F & \text{if a top view composite was involved} \\ \text{similarity} & \text{otherwise} \end{cases}$$

The bias factor F is determined by actually executing the view determination on the training set and estimating the apparent bias toward one view or the other.

5.1.5 Training and Testing

The preprocessed images are divided into two groups, according to aspect angle; the first group with aspect angles

180°, 174°, 21°, and 15°, and the second with
177°, 171°, 18°, and 12°.

The images in the first group are used for training, and those in the second group are used for testing, as follows:

For each view and aspect angle, a composite of all four targets at that view and angle is formed from images in the training set. Training, in our case, consists primarily of forming these composites. The view determination procedure can now be executed using these composites. Before executing the procedure on images in the testing set, the algorithm is applied to images in the training set. This test is used to indicate any adjustments (e.g., in the bias factor F). Then the (adjusted) procedure is tested on the images in the testing set.

The results obtained with this view determination procedure for the F-102, F-15, F-16 and F-5E are summarized in Table 4.

TABLE 4. DETERMINED VIEW

		Top	Side
Actual View	Top	14	2
	Side	1	15

Overall correct = 91 percent

6.0 THE STRUCTURAL APPROACH TO VIEW DETERMINATION

The determination of target shape using structural techniques requires that the image be decomposed into a number of parts or segments called atoms. These atoms can be sections of the contour of the figure or regions of bright scatterers called clusters or parts of the skeleton of the image. A set of intrinsic labels that represent features measured directly on the atoms is associated with each atom. For example when the picture atoms consist of regions of bright scatterers (clusters) such intrinsic labels would be the length, shape, area (size), orientation, brightness, variance of brightness, and coordinates in the image plane. In addition to these intrinsic labels, a set of external labels such as the relative position of each atom with respect to the other atoms in the image is also used.

The interpretation problem is to assign a set of identifiers, such as wing, engine, tail, fuselage, etc. to groups of atoms. Since the relative positions of these major aircraft components are known a priori, the interpretation problem is reduced to a search for a mapping from the measured set of atoms to the set of identifiers, which is consistent with the external labels. For example, if one atom is labeled tail, then none of the atoms to the rear of it could be labeled wing.

The formulation used is very similar to what a human would use. The algorithm picks out an easily distinguishable feature of the image such as the fuselage clusters and then infers the labels of the remaining clusters (atoms). This is done by labeling the remaining clusters according to their positions with respect to the fuselage.

The structural approach works very well with "good" images; good images being those which are readily interpreted by human observers. Images which are not well formed, due to either blurring or cross range aliasing or insufficient target rotational motion during image formation, are not interpreted successfully by the algorithm as developed at present. However, images which are half way between top and side view are handled consistently and interpreted as ambiguous.

The algorithm coded for this project works well on images of large swept wing aircraft such as airliners. The extension to small delta wing

fighters was not attempted because the amount of quality data for that class of target did not warrant the additional effort. Images of a DC-10, a 727, and a 707 from the NOSC radar were used to test the classifier. There were 54 images, 37 top views and 17 side views. The classifier gave the correct decision in 53 out of 54 cases; one side view of a DC-10 was classified as ambiguous.

6.1 ATOMS

The atoms mentioned above are the lowest level of information about the image used by the classifier. Individual pixels could be used as atoms but this would make the problem intractable. The atoms used in the present algorithm are the clusters of Section 3. These clusters provide non-overlapping regions of the image which can be used to determine the structure of the image itself.

The cluster properties which were used are

1. (x, y), the center of the cluster
2. (sx, sy), the major and minor axes of the clusters
3. theta, the orientation of the cluster's major axis
4. npnts, the number of points from the image in the cluster
5. m_{00}, the average intensity of the points in the cluster

There was one very important assumption made about the clusters: no two sections of the original image corresponding to different parts of the aircraft are contained in the same cluster. This means that the classifier does not have to deal with the possibility that the same atom may belong to different parts of the aircraft and therefore may have conflicting labels.

Also considered as atoms were overlapping clusters formed using the method of [9]. Four examples of these atoms are shown in Figure 20-d. One of the drawbacks of this cluster decomposition, however, is the requirement of a good contour, which is difficult to obtain from radar images. Some promising results for that problem were achieved using a method based on

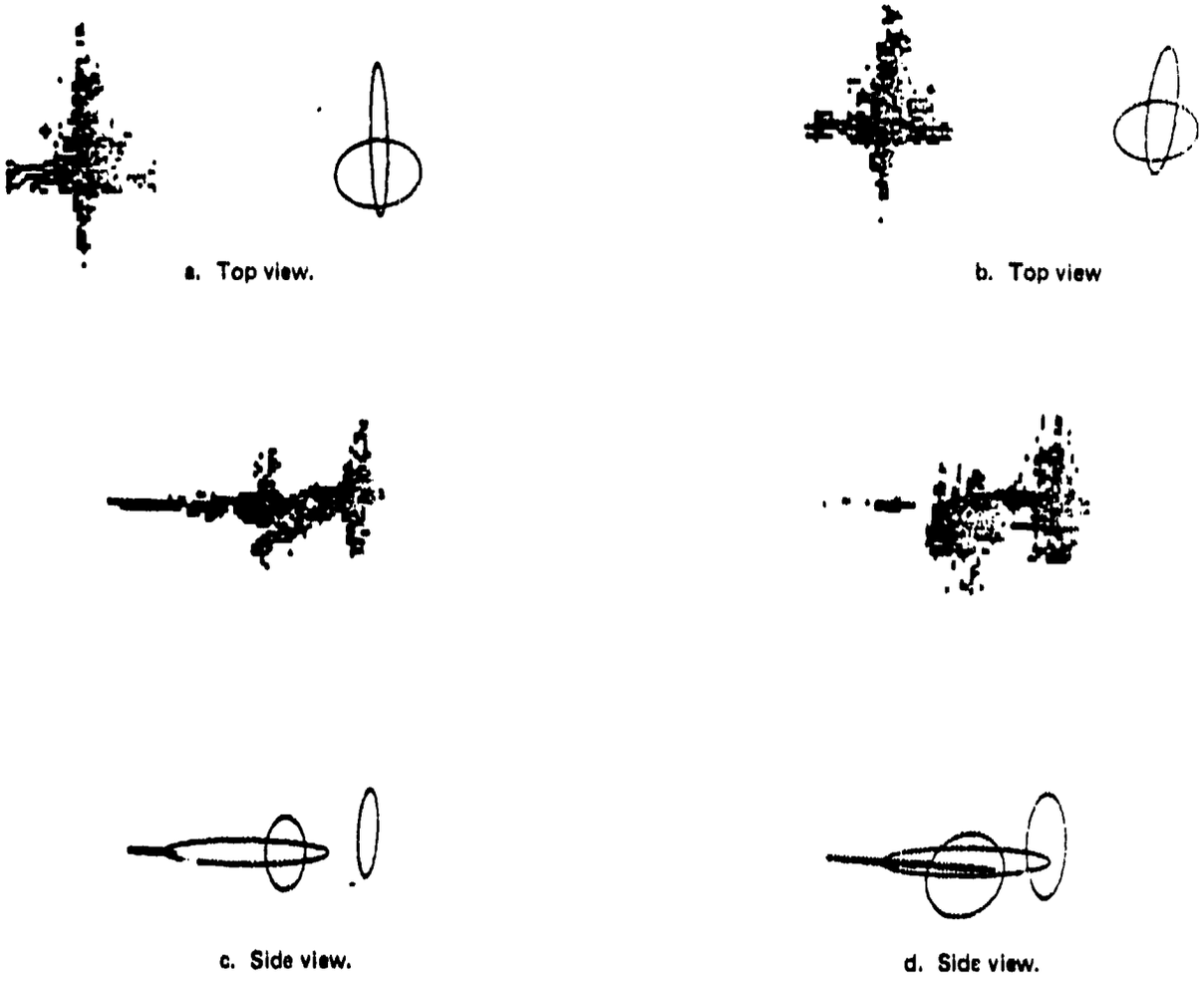

a. Top view.

b. Top view

c. Side view.

d. Side view.

Figure 20. Examples of graph theoretic clustering on the (F-5E) image contour. Ellipses are fitted to segments of the contour.

the shape hull* of a set of points but this was too sensitive to the image threshold. ISODATA the method outlined in Section 3.0, however can be made relatively insensitive to the threshold.

*The shape hull of a set of points is the boundary curve obtained from the intersection of all convex polygons formed by circumscribing the k nearest neighbors of every point with the smallest possible convex polygon; see also [10].

6.2 MODELS FOR VIEW DETERMINATION

The structural approach requires models of the possible classes against which to compare its interpretation of the image. Top and side view models of a DC-10 are shown in Figure 21.

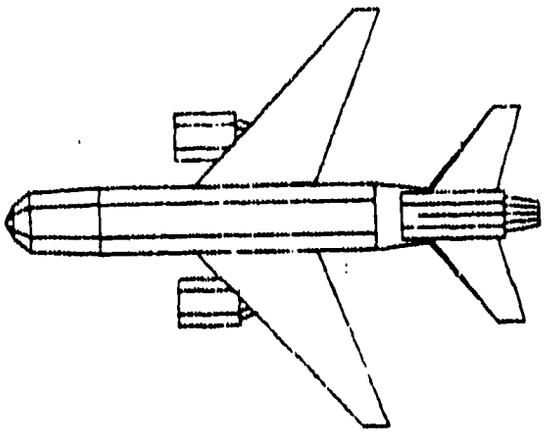

a. Top view.

b. Side view.

Figure 21. Models of a DC-10.

The main features which the classifier uses are the orientation of the wings on a top view, and the height of the tail on a side view. Other features considered are the position of the wings with respect to the nose, the symmetry of the wings about the fuselage, and the lack of one or more wings on a side view.

A DC-10 is shown in Figure 22 somewhere in between top and side view. Figure 23 shows a radar image of a DC-10 at this angle. This image was classified as ambiguous by the classifier.

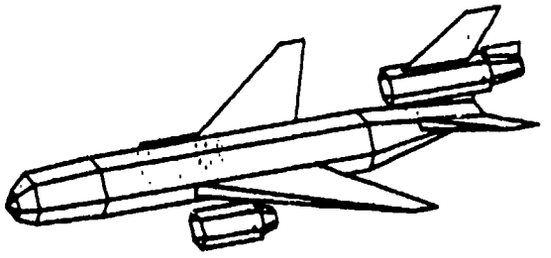

Figure 22. DC10 at angle somewhere between side and top view.

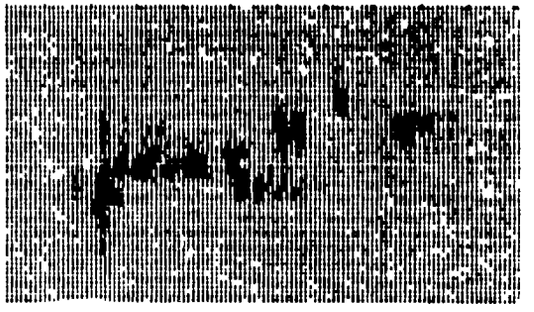

Figure 23. Radar image of a DC-10 classified as ambiguous by the classifier. (The classifier interpretation of this image corresponds roughly to Figure 22.)

6.3 RULES FOR CLUSTER LABELLING

The algorithm coded for this project requires a very rough estimate of target aspect. This allows initial labeling of the frontmost cluster, which is labelled nose, and the rearmost cluster which is labelled tail. The aspect angle estimate can be obtained by a combination of tracking data and the moments computed for the entire image using the formula:

$$\tan(2*\theta) = -2*\mu_{11}/(\mu_{20} - \mu_{02}) \tag{27}$$

as described in Section 2.

6.3.1 Fuselage Formation

The fuselage is determined by finding a set of clusters, which, when connected, form a relatively straight path from the nose to the tail. The path is found by tracing a path from the nose to the tail along an optimized minimal spanning tree. The optimized tree is formed as follows:

1. Compute the minimal spanning tree.
2. Find the path from the nose to the tail along the tree.
3. Compute the slope of the least squares line through the above path, and let $\bar{u}$ be the unit vector in that direction.
4. Compute the minimal spanning tree only for the points in the original path but with a distance function between point i and j given by

$$\begin{aligned} \text{dist} &= \text{sqrt}((xi - xj)**2 + (yi - yj)**2) \\ &\quad + 1.5*|\bar{u} \times (xi - xj,\ yi - yj)| \end{aligned} \tag{28}$$

This makes the branches of the tree tend towards the direction of the least squares line. The fuselage is then traced along the resulting tree. An example of an optimized path is shown in Figure 24.

a. Non-Optimized

b. Optimized

Figure 24. Path from nose to tail clusters. Dotted lines show the minimal spanning tree.

6.3.2 Wing Location

After the final fuselage is obtained, another least squares line is fit to it. This least squares line is given in point slope form as:

$$(y - y_o) = b(x - x_o) \tag{29}$$

This line divides the plane into two half planes. The discriminant

$$d = b \cdot (x - x_o) + y_o - y \tag{30}$$

gives positive values in one half and negative in the other. In this manner the clusters which are not on the fuselage are divided into two disjoint sets. From these sets the wing are formed. Before the wings are formed, however, the sets are pruned according to the following set of rules:

let r be the radius of gyration = $\sqrt{\mu_{20} + \mu_{02}}$ (see also Equation (6)) (31)

1. if the distance from a cluster to its closest neighbor is >1.5*r then delete the cluster from the wing set.
2. if a cluster is deleted from a wing set then it is attached to the nearest fuselage cluster.

After the sets have been pruned, then the wings are formed in the following manner:

1. compute a minimal spanning tree on the points in the set.
2. trace the path along that tree from the base of the wing to the tip.

The base and the tip of the wing are defined as follows:

> The base of the wing is the cluster closest to the point (Xc, Yc) which is the point of intersection of the perpendicular through the center of the wing set and the fuselage line. (See Figure 25)

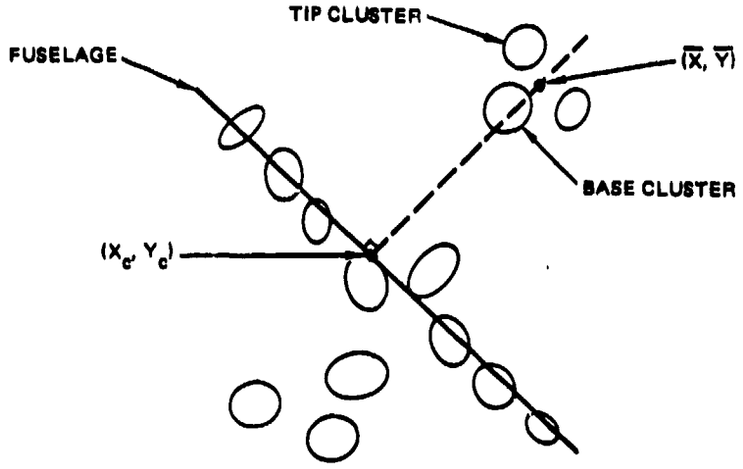

Figure 25. Example of locating wing clusters.

> The tip is defined to be that cluster in the set which is furthest from the fuselage line.

The wings found by the above method are then pruned and reformed to ensure that all spurious clusters have been removed.

6.3.3 Unbound Cluster Labelling

After the formation of the fuselage and the wings, there may be atoms which have not been given any label. These unbound clusters fall into two categories, noise clusters and clusters which belong to the fuselage and wings.

The algorithm for labeling the unbound clusters can be described by the following four steps:

1. Use a least squares straight line fit through the fuselage clusters of the form

$$(y - y_o) = a \cdot (x - x_o)$$

2. For every unbound cluster with cluster center coordinates (x_c, y_c) compute the linear discriminant functions

$$d = a(x_c - x_o) - (y_c - y_o)$$

and depending on the sign of d assign the cluster to either the left or the right wing.

3. Project the cluster center onto the fuselage. If the projections do not lie between the nose and the tail the cluster is left unbound, otherwise proceed to the next step.

4. Compute the distance d_w from the center of the cluster under consideration to the centroid of all the wing clusters. Also compute its distance d_f to the fuselage line. If $d_w < d_f$, assign the cluster to the wing; else if $d_f < 0.25$ x (distance from nose to tail), assign the cluster to the fuselage; otherwise, the cluster remains unbound.

6.3.4 Engine Detection

One of the significant features of aircraft radar images is the number and location of the engines. During this project an algorithm was developed which identified certain clusters as engine clusters even though this information was not used in the determination of target view. Furthermore the only engine detection attempt that was made was to find engines on the wings using only the relative position of engine clusters with respect to the wing and fuselage clusters. The present algorithm can be improved by including such internal cluster characteristics as density, brightness, texture and orientations. However even without these more sophisticated detection criteria the present algorithm successfully identified some of the engines on images of a DC-10 and a 707, examples of which are shown in Figure 26.

a. DC–10

b. 707

Figure 26. Results of labelling. (Beside each image is the line drawing derived from the labels assigned. Stars mark the positions of clusters designated as engines.)

6.4 DECISION ALGORITHM

Once the clusters have been labelled, classification as a top or side view is a matter of choosing the right features based on geometric relations among the aircraft parts and deciding according to these. Five features were used to make the classification.

6.4.1 Wing Orientation

The orientation of each of the wings with respect to the fuselage was measured by representing each part by a vector as in Figure 27 and computing,

$$\theta = \cos^{-1}(\vec{f}\cdot\vec{w}/(|\vec{f}|\ |\vec{w}|)) \qquad (32)$$

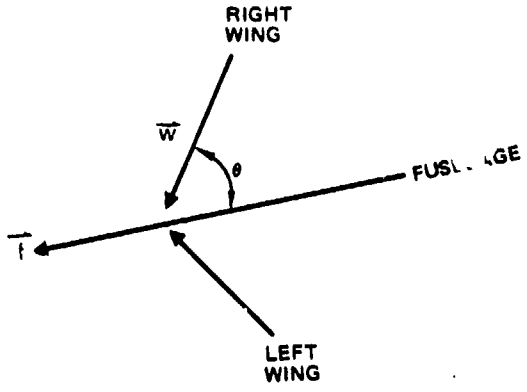

Figure 27. Wing and fuselage shown as vectors in a plane.

Using the angle θ for the left and right wings a parameter N_w was computed by counting the number of wings with proper orientation where proper orientation was defined to be such that $\pi/9 < \theta < \pi/2$.

6.4.2 Angle of Symmetry

The angle of symmetry of the wings about the fuselage was also computed by drawing a vector between the centers of the two wings as shown in Figure 28 and computing the angle

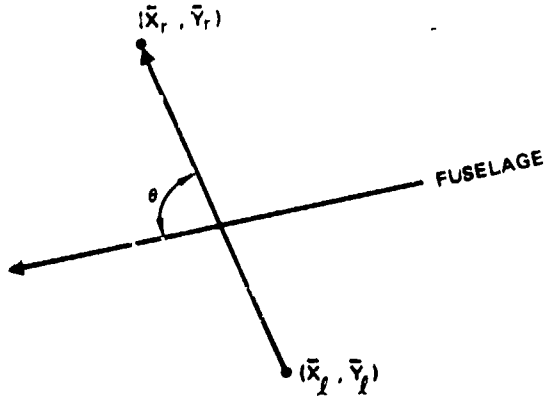

Figure 28. The angle between the line between the wings and the fuselage was also used as a feature.

$$s = 90 - (180/\pi)*\theta \tag{33}$$

which ranges between -90 and 90, 0 being perfect symmetry.

6.4.3 Balance Factor

The balance of the wings about the center of the fuselage was also used as a feature. Two distances d1 and d2 were computed as shown in Figure 29 and the balance factor b defined by

$$b = 2*(1/2 - d1/d2) \tag{34}$$

was computed. This factor ranges from -1 to 1, 0 being perfect balance.

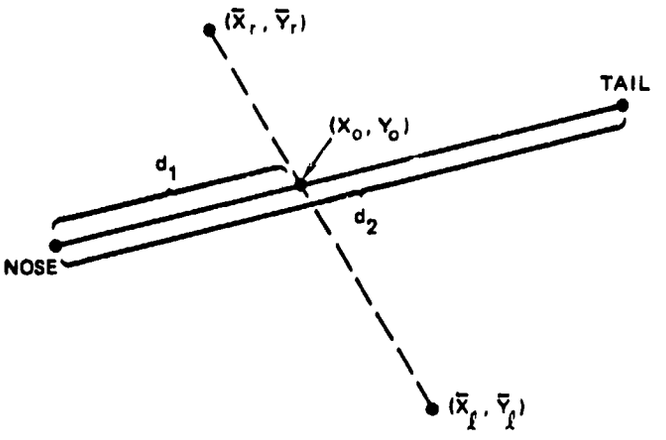

Figure 29. Distances measured to compute the balance factor.

6.4.4 Boolean Features

Two binary features, w and t, describing the wings and tail were computed as follows;

> if either of the wings is missing then w = true
> else w = false
>
> if the tail extends further from the fuselage than both wings then t = true
> else t = false

6.4.5 Classification Rule

After the above features are computed the following rules are used to classify each image as a top, a side, or an ambiguous view.

if w is true then SIDE
else if $N_{w'} = 2$ and not t then TOP
else if $N_{w'} = 2$ then AMBIGUOUS
else if $|s| < 30$ and not t and $N_{w'} > 0$ then TOP
else if $|s| < 10$ and $N_{w'} > 0$ and $|b| > 1/4$ then TOP
else SIDE

6.5 SUMMARY OF CLASSIFICATION RESULTS

The program for this method was tested on 54 of the images obtained from the NOSC radar, broken down as follows:

DC-10 top views 10 images
DC-10 side views 9 images
727 top views 15 images
727 side views 3 images
707 top views 12 images
707 side views 6 images

These "good" images were chosen from the data available because they were such that a human observer might be able to identify them. The structural approach does not do well on other images because it is based on human like classification rules.

All of the 37 top views were identified by the classifier. Of the 17 side views, only one was declared ambiguous (see Figure 33).

Figures 30 through 37 show some examples of cluster labeling of the ISODATA clusters, using the methods described above. These figures show that although considerable success has been achieved with the above methods there is still a need to refine and improve the techniques.

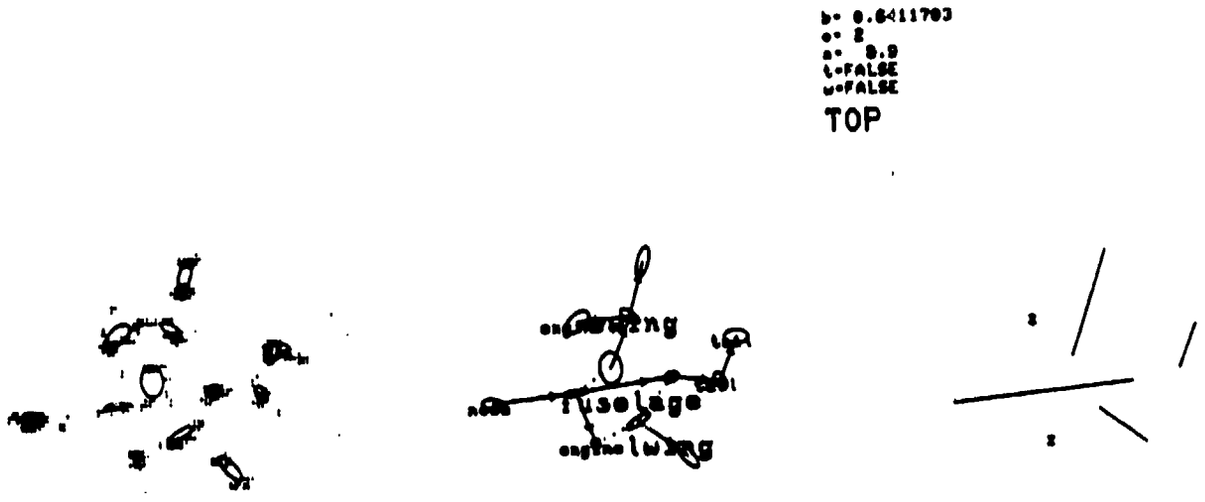

Figure 30. Successful labeling of DC-10 top view.
(Note the engine detection and tail formation).

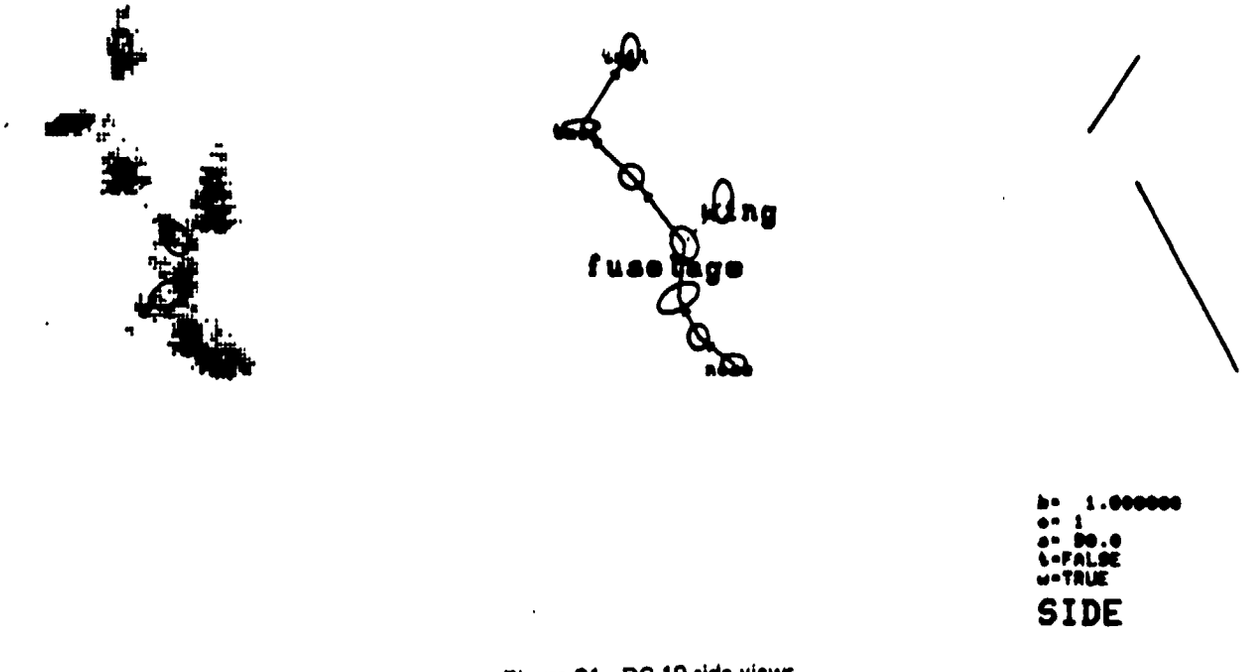

Figure 31. DC-10 side views.

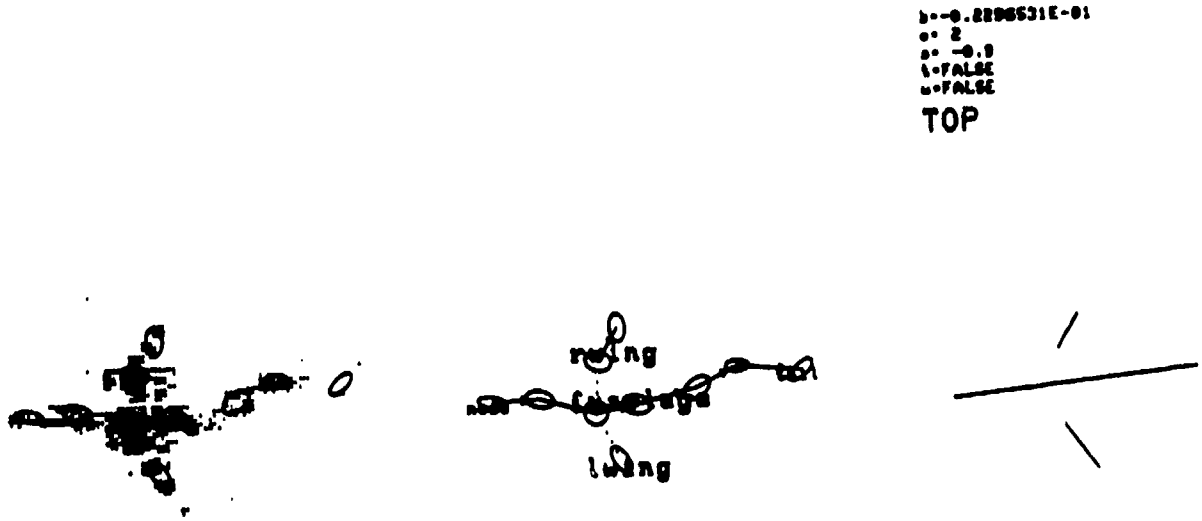

Figure 32. 727 image (top view with almost perfect features: balance, wing orientation, and symmetry.)

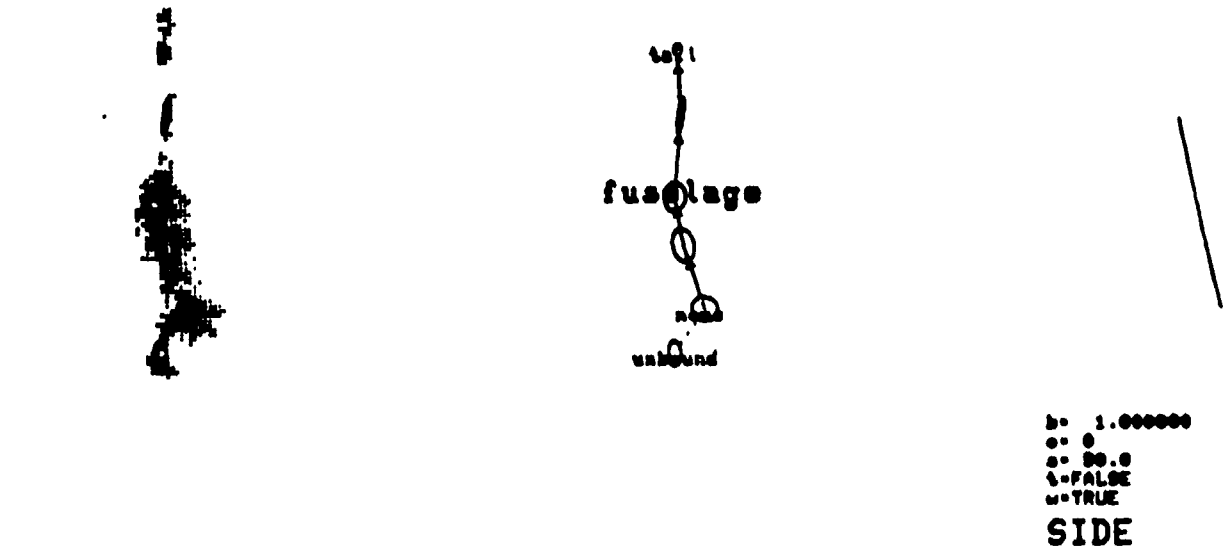

Figure 33. 727 side views.

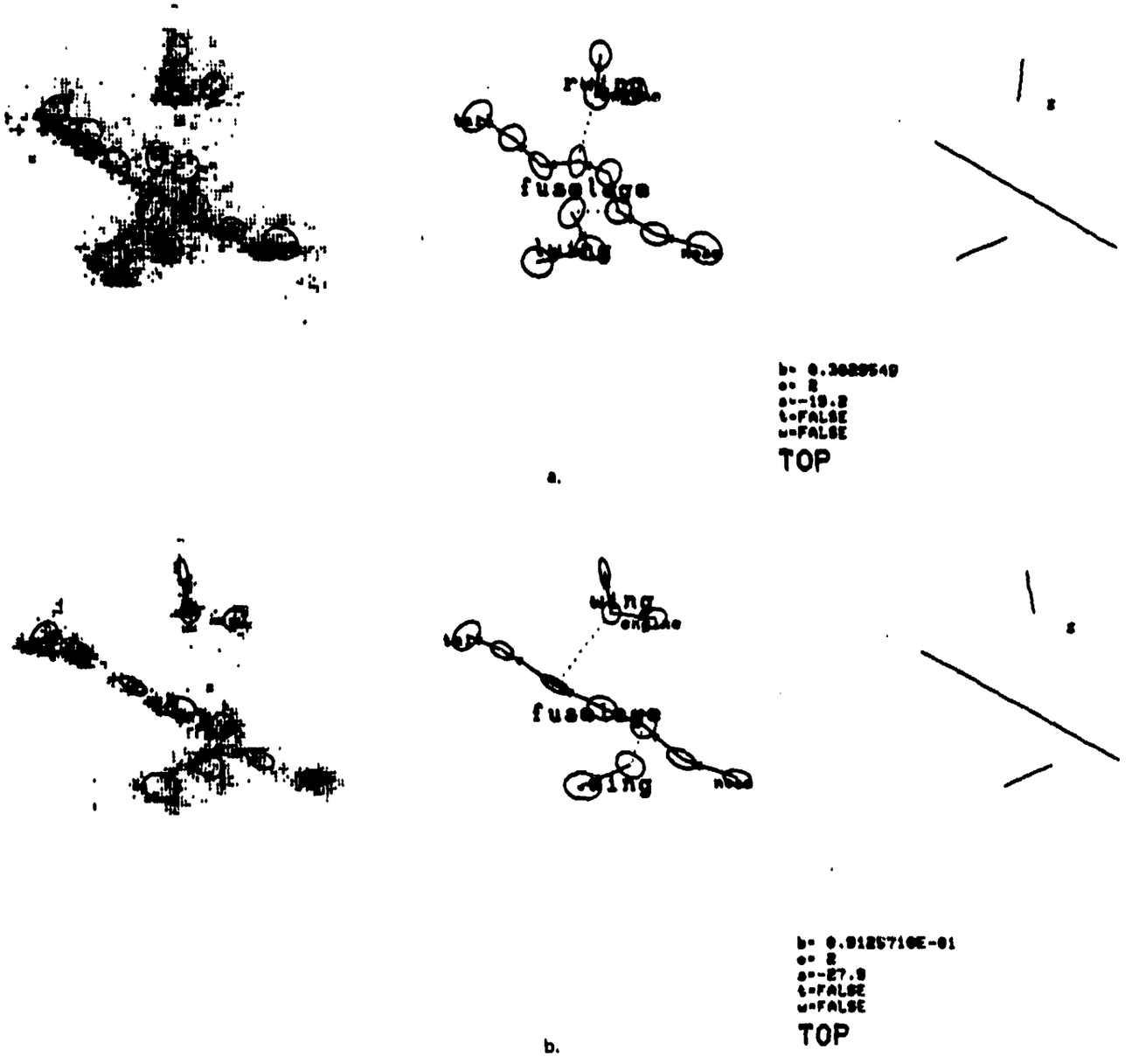

Figure 34. Results of labeling 707 top views. (Show the need for improving the engine detection scheme.)

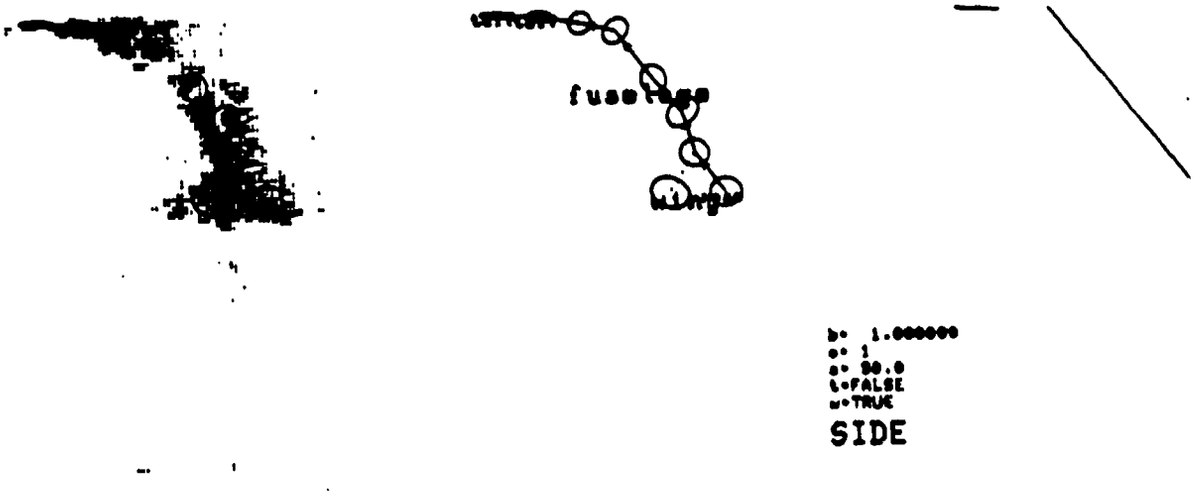

Figure 35. Side view of 707 which matches the prototype exactly.

7.0 VIEW DETERMINATION USING MOMENTS – A STATISTICAL PATTERN RECOGNITION APPROACH

Both the syntactic and structural approach to view determination discussed above were based on recognizing a consistent and repetitive pattern present in either top or side view images of aircraft targets. In a statistical pattern recognition approach a set of numerical features is computed from the image and used to form a feature vector. A training set of feature vectors from top and side view images is then used to construct a statistical classifier. Using cluster decomposition of the aircraft radar images geometric moments were computed by considering the center of each cluster as a point with mass equal to the total cluster intensity. All moments with orders 2 to 6 (a total of 25) were used to form a feature vector. Using feature vectors from a training set of top and side view images for nose and tail aspects of the five RATSCAT targets (F-102, F-15, F-16, F-SE and A-10) a Gaussian classifier was constructed to recognize target view. The performance of the classifier on the RATSCAT images is shown in Figure 36. As seen

CLASSIFIER DECISION

TARGET VIEW		TOP VIEW	SIDE VIEW
	TOP VIEW	28	2
	SIDE VIEW		19

NOSE ASPECTS

CLASSIFIER DECISION

TARGET VIEW		TOP VIEW	SIDE VIEW
	TOP VIEW	23	7
	SIDE VIEW	2	28

TAIL ASPECTS

Figure 36. View determination using moments computed after cluster decomposition of radar images of the five RATSCAT targets, (F-102, F-15, F-16, F-5E, A-10) using separate training and testing sets.

in this figure a 78 percent correct view determination was achieved for nose aspects and 85 percent for tail aspects. A Gaussian classifier was also used to classify the individual targets after view determinations using moments computed after cluster decomposition of the radar images. The resulting classifications performance was 71 percent correct for nose aspects and 80 percent correct for tail aspects for images classified as top views. For images classified as profiles by the automatic classifier, the identification rate was 57 percent correct and 60 percent correct for nose and tail aspects respectively. These classification results are tabulated on a per target basis in Figure 37. A classification test was also performed on the combined data set of top and side view images without view determinations. Instead the classification was performed for a ten class problem: F-102 top and side, F-15 top and side, F-16 top and side, F-5E top and side, and A-10 top and side. The results shown in Figure 38 were 44 percent correct for nose aspects and 38 percent correct for tail aspects. These results indicate that for the RATSCAT targets considered above there are common features among the top views of all the targets which are significantly different from similar features for side views. A classification test combined with view determination was also performed on the combined data set of RATSCAT and NOSC targets. Because the aspects for many of the NOSC targets were broadside while those for the RATSCAT targets were nose or tail, an aspect independent feature vector (such as the one computed from the invariant moment functions) was used for this test. All images from each target were grouped without regard to aspect. Further because the number of images from the NOSC data was too small to allow splitting into training and testing, the same images were used for both training and testing. All targets were treated equally for this test by using the same RATSCAT imager for training and testing on each target and by combining the nose and tail aspects into one aspect angle sector. The results of this combined nine class test were 78 percent correct for those images classified as top views and 70 percent correct for those images classified as side views. These results are shown in Figure 39,

CLASSIFIER DECISION

TARGET PRESENT

	F102	F15	F16		A10
F102	6	3			
F15		6			
F16	3	1	3		
F5E				7	
A10		4			5

71% CORRECT
0% UNKNOWN

CLASSIFIER DECISION

TARGET PRESENT

	F102	F15	F16	F5E	A10
F102	2				
F15	1	1	1	1	2
F16		1	4		
F5E		1	1	2	1
A10					3

57% CORRECT
0% UNKNOWN

NOSE ASPECTS

CLASSIFIER DECISION

TARGET PRESENT

	F102	F15	F16	F5E	A10
F102	3	1			
F15		4	2		1
F16			5		
F5E			1	5	
A10					3

80% CORRECT
0% UNKNOWN

CLASSIFIER DECISION

TARGET PRESENT

	F102	F15	F16	F5E	A10
F102	5			3	
F15		2	1	1	1
F16			5	2	
F5E				4	2
A10		2	1	1	5

60% CORRECT
0% UNKNOWN

TAIL ASPECTS

CLASSIFICATIONS OF IMAGES CLASSIFIED AS TOP VIEWS

CLASSIFICATION OF IMAGES CLASSIFIED AS PROFILES.

Figure 37. View determination followed by classification using moments computed after cluster decomposition separate training and testing sets.

CLASSIFIER DECISION

TARGET PRESENT	F102	F15	F16	F5E	A10	UKN
F102	3		1	4	3	
F15			5	3	4	
F16		1	6	4	1	
F5E			2	7	3	
A10			1	1	10	

44% CORRECT
0% UNKNOWN

NOSE ASPECTS

CLASSIFIER DECISION

TARGET PRESENT	F102	F15	F16	F5E	A10	UKN
F102	2		6	1	3	
F15	1	3	3	1	4	
F16		1	7	1	3	
F5E	1		2	7	2	
A10			4	4	4	

38% CORRECT
0% UNKNOWN

TAIL ASPECTS

Figure 38. Classifications of a combined set of top and side view images using moments after cluster decomposition. Data are treated as a ten class problem for these tests i.e., F-102 top and side, ... A-10 top, and side.

CLASSIFIER DECISION

TARGET PRESENT	F102	F15	F16	F5E	A10	DC10	727	707	A3	UKN
F102	10	1		2					1	3
F15		11		2					1	
F16	2		6				1		1	2
F5E		4		10					1	2
A10			1		14		1			5
DC10						10		1		
727						2	12			
707						1	2	12		
A3	1								6	6

78% CORRECT
13% UNKNOWN

CLASSIFICATION OF IMAGES CLASSIFIED AS TOP VIEWS

CLASSIFIER DECISON

TARGET PRESENT	F102	F15	F16	F5E	A10	DC10	727	707	A3	UKN
F102	9		5			1	1			3
F15	5	13	1	1			1			1
F16	1		11	5			2			5
F5E	1		1	13					2	2
A10					11				4	
DC10						8				
727			1	1			2			
707								3		
A3									7	

70% CORRECT
9% UNKNOWN

CLASSIFICATION OF IMAGES CLASSIFIED AS SIDE VIEWS

Figure 39. View determination followed by classification using invariants computed after cluster decomposition (training and testing are the same, nose and tail aspect images are mixed).

8.0 CONCLUSIONS

Summarizing the results presented in the previous sections, it can be observed that in general view determination of relatively good aircraft radar images is possible and tends to improve classification. Since this investigation was primarily concerned with algorithm development, the work concentrated on relatively 'good' images. The problem, however, is that the majority of radar images of aircraft targets are not 'good' so that many of the techniques discussed here may either fail completely or have their performance significantly reduced.

In general the syntactic and structural techniques described here will most likely fail completely on bad images. For example the syntactic scheme developed here gave an 89 percent correct view determination for good images of the DC-10, 727 and 707 but using relatively good images of the RATSCAT targets the technique yielded a success rate which was only 25 percent better than random guessing. The structural scheme which attempts to interpret images in a human like manner is also very sensitive to image quality. In principle much more elaborate rule based schemes could be attempted than the one described in Section 6.0 to interpret bad or ambiguous aircraft radar images. However, since ISAR images depend on target motion it may be more advantageous to investigate the use of collateral tracking information for aspect and possible view determination. The results of this investigation also show that statistical pattern recognition schemes using moments yield results which are at least as good as the results achieved with some of the more elaborate syntactic and structural techniques developed during this study. Thus it seems that until the quality of aircraft radar images improves considerably, statistical pattern recognition schemes will provide the most efficient aircraft radar image classification algorithms.

9.0 REFERENCES

1. Dudani, S. A., Breeding, K. J., and McGhee, R. B., Aircraft Identification by Moment Invariants, IEEE Trans. On Computers, Vol. C-26, pp. 39-45, 1977.
2. Hu, M. K., Visual Pattern Recognition by Moment Invariants, IRE Trans. On Inf. Theory, pp. 179-187, 1962.
3. Gonzales, R. C., and Moret, B. M. E., A Recursive Procedure for Updating Quadratic Forms and Its Application to Feature Selections, ONR-CR215-288-3F, 1978.
4. Ioannidis, "Target Identification Using Radar Imagery and Moment Methods," Hughes Aircraft N00014-79-C-0643.
5. Ball, G. H., and Hall, J. J., "ISODATA, An Iterative Method of Multivariate Data Analysis and Pattern Classification," Proc. IEEE Int. Commun. Conf., June 1966, pp. 116-117.
6. Ball, G. H., and Hall, D. J., "ISODATA, A Novel Technique for Data Analysis, and Pattern Classification," Technical Report, Stanford Research Institute, Menlo Park, California, May 1965.
7. Coleman, G. B. and Andrews, H. C., Image Segmentation by Clustering, Proceeding of the IEEE, Vol. 67, May 1979, pp 773-785.
8. Meisel, W. S., Computer-Oriented Approaches to Pattern Recognition, Academic Press, NY, 1972.
9. Shapiro and Haralick, "Decomposition of Two-Dimensional Shapes by Graph Theoretic Clustering," IEEE Tans Pattern Analysis, Vol. PARMI-1, No. 1, January 1979.
10. Jarvis, "Computing the Spape Hull of Points in the Plane," Dep. of Com. Sci., Australian Nat. Univ.

APPENDIX

SYNTACTIC PATTERN RECOGNITION

Syntax refers to the structure of sentences in a language as described by a grammar. The grammar can be defined as a set of rules for constructing (grammatically correct) sentences. A formal grammar is defined similarly as a finite set of rules for generating the sentences of the associated language (a formal language is simply a set of sentences).

In a syntactic approach to pattern recognition, an analogy is made between patterns in a class and sentences in a language. By analogy, each pattern in a given class is generated by a "grammar" associated with that class. The syntactic pattern recognition task is then

1. To find the grammar from a set of patterns known to be in the class
2. Given an unclassified pattern, check if it can be constructed from the grammar. If so it is in the associated class.

Formally, a formal grammar is defined as a triple (X, N, T, P) where N and T are mutually exclusive, finite sets of symbols. The symbols in N are called non-terminals, and those in T are called terminal symbols. X is a symbol in N, and is called the "initial nonterminal," or the "start symbol". P is a set of "production rules", which are essentially pairs of strings composed of symbols in $|T| \cup |N|$. Such a production rule is denoted as

$$x \longrightarrow y$$

where: x and y are a pair of strings.

The productions are interpreted or used as rules for generating the strings in the set represented by the given grammar. "Application" of a production rule

$$x \longrightarrow y$$

as above, to an arbitrary string Z consists of finding a substring of Z identical to x, and replacing it with y. This forms a new string from Z.

A string Z, is said to be derived in one step from another string Z_o if there is a production x → y of the grammar which, when applied to Z_o, results in Z_1. This is called a one step derivation and is denoted by

$$Z_o \overset{1}{\Rightarrow} Z_1$$

The notion of a derivation is then extended to any number of steps by stipulating that

$$Z \overset{o}{\Rightarrow} Z$$

and if $Z \overset{n}{\Rightarrow} Z^1$, and $Z^1 \overset{1}{\Rightarrow} Z''$ then $Z \overset{n+1}{\Rightarrow} Z''$, where Z, Z^1, and Z'' are strings of symbols in {T} U {N}.

The set of strings generated by the given grammar is defined as {Z | Z is a string of symbols in T, and $X \overset{n}{\Rightarrow} Z$ where n is any non-negative integer and x is the start symbol.}

The concept of a grammar can be extended from strings to more general graph structures, tree structures for example as described in [2]. Also, the production rules can be generalized to "probabilistic" productions, in which a production

$$x \xrightarrow[p]{} y$$

denotes that x would get replaced by y with probability p. For a more detailed presentation of probabilistic grammars and syntactic pattern recognition see [1], [2].

Given a string and a grammar, "parsing" the string refers to finding its derivation from the start symbol, in accordance with the given grammar.

To summarize, syntactic pattern recognition attempts to describe each class of patterns under consideration as a set generated by the same grammar: An unclassified pattern is then classified in the class or set corresponding to the grammar in which the given pattern can be parsed successfully, or with the greatest probability in the case of probabilistic grammars.

REFERENCES

[1] Gonzalez, R. G. and Thomason, M. G., Syntactic Pattern Recognition, Addison-Wesley, 1978.

[2] Fu K. S., Syntactic Methods in Pattern Recognition Academic Press, 1974.

DISTRIBUTION

Addressee	DODAAD Code	Number of Copies
Scientific Officer	N0014	1
Administrative Contracting Officer	FY1767	1
Director, Naval Research Laboratory Attn: Code 2627 Washington, D.C. 20375	N00173	6
Defense Technical Information Center Bldg. 5, Cameron Station Alexandria, VA 22314	S47031	12
Office of Naval Research, Western Regional Office 1030 East Green Street Pasadena, CA 91106	N62887	1